The single-cell atlas of the murine reproductive tissues during preterm labor

Valeria Garcia-Flores[1,2], Roberto Romero[1,3-7], Azam Peyvandipour[1-3], Jose Galaz[1,2], Errile Pusod[1,2], Bogdan Panaitescu[1,2], Derek Miller[1,2], Yi Xu[1,2], Li Tao[1,2], Yesong Liu[1,2], Adi L. Tarca[1,2,8], Roger Pique-Regi[1-3,*], Nardhy Gomez-Lopez[1,2,9,*]

[1]Perinatology Research Branch, Division of Obstetrics and Maternal-Fetal Medicine, Division of Intramural Research, *Eunice Kennedy Shriver* National Institute of Child Health and Human Development, National Institutes of Health, U.S. Department of Health and Human Services (NICHD/NIH/DHHS); Bethesda, Maryland, and Detroit, Michigan, USA.

[2]Department of Obstetrics and Gynecology, Wayne State University School of Medicine; Detroit, Michigan, USA.

[3]Center for Molecular Medicine and Genetics, Wayne State University; Detroit, Michigan, USA.

[4]Department of Obstetrics and Gynecology, University of Michigan; Ann Arbor, Michigan, USA.

[5]Department of Epidemiology and Biostatistics, Michigan State University; East Lansing, Michigan, USA.

[6]Center for Molecular Medicine and Genetics, Wayne State University; Detroit, Michigan, USA.

[7]Detroit Medical Center; Detroit, Michigan, USA.

[8]Department of Computer Science, Wayne State University College of Engineering; Detroit, Michigan, USA.

[9]Department of Biochemistry, Microbiology, and Immunology, Wayne State University School of Medicine; Detroit, Michigan, USA.

24

25 ***Correspondence**

26 Nardhy Gomez-Lopez, MSc, PhD, Department of Obstetrics and Gynecology, Wayne State
27 University School of Medicine, Perinatology Research Branch, NICHD/NIH/DHHS, 275 E.
28 Hancock, Detroit, Michigan 48201, USA. Tel: (313) 577-8904. Email: nardhy.gomez-
29 lopez@wayne.edu
30 Roger Pique-Regi, PhD, Center for Molecular Medicine and Genetics, Department of Obstetrics
31 and Gynecology, Wayne State University School of Medicine, 540 E. Canfield Ave., Detroit,
32 Michigan, 48201, USA. Tel: (313) 577-0719. Email: rpique@wayne.edu

33

ABSTRACT

Preterm birth, the leading cause of perinatal morbidity and mortality worldwide, frequently results from the multi-etiological syndrome of preterm labor. Intra-amniotic infection is the best-established causal link to preterm labor and birth, and involves the premature activation of the parturition cascade in the reproductive tissues (uterus, decidua, and cervix). However, the simultaneous investigation of the cellular landscape and interaction networks in such tissues at single-cell resolution had not been undertaken. Herein, we utilized scRNA-seq to reveal that preterm labor affects the cellularity of the uterus, decidua, and cervix through immune cell infiltration and altered transcriptomic profiles of non-immune cell types. Preterm labor-affected cells showed shared and distinct immune processes, the latter indicating tissue-specific cellular functions. Cell-cell communication analysis implicated immune and non-immune cell types in preterm labor-associated inflammatory pathways across tissues. Next, correlation between uterine transcriptomic data from mice with local or systemic inflammation-induced preterm labor indicated significant overlap in labor-associated gene expression. Last, comparison of cell-cell communication in the murine and human uterus revealed shared signaling pathways implicated in preterm and term parturition. Together, these findings provide novel insight into the cellular landscape, dynamics, and communications in the reproductive tissues during preterm labor leading to premature birth.

INTRODUCTION

Preterm birth is a devastating clinical condition that affects 15 million infants each year and is the leading cause of neonatal morbidity and mortality worldwide [1, 2]. Spontaneous preterm birth often results from preterm labor, a syndrome for which multiple etiologies have been proposed [3, 4]. Among these, the best-established causal link to preterm birth is intra-amniotic infection, a clinical condition resulting from the invasion of microbes into the amniotic cavity [5-13]. The most frequently detected bacteria in amniotic fluid of women diagnosed with intra-amniotic infection include genital mycoplasmas, *Streptococcus agalactiae*, *Gardnerella vaginalis*, and *Escherichia coli*, among others [14-25]. Human descriptive studies have consistently shown that such microbial invasion of the amniotic cavity is accompanied by a local acute inflammatory response that includes the infiltration of leukocytes into the amniotic cavity (inc. amniotic fluid [26-39] and placental tissues [40-57]) as well as the reproductive tissues [58, 59]. More recently, animal models coupled with omics technologies have been utilized to strengthen this concept and establish causality between intra-amniotic infection and the inflammatory milieu observed in the reproductive tissues (e.g., uterus, decidua, and cervix) that serve to orchestrate the premature activation of the common pathway of labor [60-63]. However, the simultaneous investigation of the cellular landscape and interaction networks at single-cell resolution in the intrauterine components responsible for preterm parturition has not been undertaken.

Single-cell technology has emerged as a useful tool for evaluating cellular composition, transcriptomic activity, and communication networks in gestational and reproductive tissues [64-70]. Indeed, we have applied single-cell RNA-sequencing (scRNA-seq) to investigate the physiological and pathological processes of labor in the placenta and extraplacental membranes

[69]. More recently, we utilized scRNA-seq to unravel the myometrial cell types that participate in the normal process of term parturition as well as key cell-cell interactions taking place in this compartment [71]. Importantly, the discovery of single-cell signatures derived from the placental tissues and myometrium possesses translational value as these can serve as potential non-invasive biomarkers of labor progression and/or obstetrical disease [66, 69, 71-74].

In the current study, we utilized scRNA-seq coupled with an allogeneic murine model of intra-amniotic infection to investigate the cellular landscape and cell-cell communications in the reproductive tissues (uterus, decidua, and cervix) during the process of preterm labor. First, we utilized a high-resolution ultrasound system to establish a murine model of preterm labor and birth induced by the intra-amniotic inoculation of *E. coli* and, using the same system, we established the timing of active preterm labor by assessing cervical shortening. Next, using scRNA-seq and computational approaches, we generated a single-cell atlas of the uterus, decidua, and cervix during preterm labor as well as their cell type-specific transcriptomic activity. In addition, we established the cell-cell communication networks between cell types in each tissue during preterm labor. Moreover, we compared the uterine transcriptomic changes induced by local or systemic inflammation leading to preterm labor and birth. Lastly, we integrated cell-cell signaling pathways between the murine uterus and the human myometrium during the processes of preterm and term labor, respectively.

RESULTS AND DISCUSSION

A single-cell atlas of the murine reproductive tissues during preterm labor induced by *E. coli*

Intra-amniotic infection has been documented as inducing inflammatory changes in the tissues surrounding the amniotic cavity [75-78]. To investigate such changes at single-cell resolution, we first established a murine model of preterm labor and birth induced by the intra-amniotic inoculation with *E. coli*, a microorganism commonly identified in the amniotic fluid of women with intra-amniotic infection [14, 16, 20, 79]. Mice with an allogeneic pregnancy underwent ultrasound-guided intra-amniotic injection of *E. coli* or vehicle control on 16.5 days *post coitum* (dpc) (Figure 1A). Intra-amniotic inoculation with *E. coli* reduced gestational length in the majority of dams (Figure 1B), resulting in an 83.3% (5/6) rate of preterm birth (Figure 1C). To evaluate the timing of preterm labor, we intra-amniotically injected a second cohort of mice with *E. coli* or PBS and utilized ultrasound to evaluate cervical length just prior to intra-amniotic injection and again 24 h later as a readout of cervical effacement (Figure 1D). Cervical length was diminished in all dams that received intra-amniotic *E. coli* at 24 h post-injection, indicating that these dams were in active preterm labor, whereas cervical length was unaltered in controls (Figure 1E). Histological analyses revealed that the induction of preterm labor was accompanied by collagen degradation in the uterine and cervical tissues (Figure 1-figure supplement 1A-C). Therefore, intra-amniotic inoculation with *E. coli* represents a translational model that resembles the clinical scenario of intra-amniotic infection leading to preterm labor and birth.

Preterm parturition includes the activation of the common pathway of labor that comprises increased uterine contractility, the triggering of local immune response in the decidual

tissues, and cervical dilatation [4, 80-84]. Therefore, to establish a single-cell atlas of the reproductive tissues in preterm labor, we collected the uterus, decidua, and cervix of dams that received intra-amniotic inoculation with *E. coli* or control on 17.5 dpc (during preterm labor induced by *E. coli*) and generated single-cell suspensions for single-cell RNA-sequencing (scRNA-seq) (Figure 1F). The uniform manifold approximation and projection plot (UMAP) in Figure 1G highlights the heterogeneous and distinct cellular composition of the uterus, decidua, and cervix. Overall, 31 cell types were identified across the uterus, decidua, and cervix: smooth muscle (2 clusters), epithelial (10 clusters), fibroblast (3 clusters), stromal (3 clusters), Endothelial, Neutrophil, Monocyte, macrophage (2 clusters), Dendritic Cell, T cell, B cell, NK cell (2 clusters), Erythroid, Plasmocyte, and Trophoblast (Figure 1H). The uterus, decidua, and cervix each displayed a distinct basal (control) cellular repertoire: the uterus showed a predominance of fibroblast (clusters 0 and 1) and non-decidual stromal (clusters 2 and 12) cell types, whereas the decidua also included a unique subset of stromal cells (cluster 4) in addition to the abovementioned cell types (Figure 1I). The uterus and decidua of control mice also included modest populations of innate immune cells such as Monocyte and macrophage subsets as well as lymphocytes such as T cell, NK cell-1, NK cell-2, and B cell (Figure 1I), likely representing the resident immune populations that have been characterized in human and murine tissues [67, 69, 71, 85-88]. By contrast with the uterus and decidua, the cervix of control mice comprised a diverse compartment of epithelial subsets (clusters 5, 7, 8, 10, 11, 14) and other major cell types (Figure 1I), as previously shown [89-91]. Immune cells were largely scarce in the cervix as well, although a modest Macrophage-1 population was observed (Figure 1I) that is consistent with prior reports of cervical cell composition in late gestation [92-95].

138 During preterm labor, an increase in innate immune cells such as Monocytes,
139 macrophages, Dendritic cells, and Neutrophils (clusters 3, 6, 9, and 18) was observed in the
140 uterus, decidua, and, to a lesser extent, the cervix (Figure 1J). Notably, the T cell population
141 (cluster 16) was also observed to increase in the uterus and decidua in preterm labor (Figure 1J),
142 which is consistent with prior studies implicating T-cell infiltration and activation as a
143 component of parturition [96-103]. Interestingly, a subset of epithelial cells (cluster 11,
144 Epithelial-10) that was largely absent in the uterus and decidua of controls became apparent in
145 preterm labor (Figure 1J). We also evaluated whether cells of fetal origin were represented
146 among the populations of the uterus, decidua, and cervix during preterm labor (Figure 1K-M). A
147 small population of fetal cells (Trophoblasts) was detected in the uterus and decidua, which is
148 consistent with prior single-cell studies of the human myometrium [71] and may represent
149 residual placental cells attached to the uterus and decidua.

150 To further explore changes in cell type composition, we examined the effects of preterm
151 labor on the abundance of each cell type identified across all tissues (Figure 2A) as well as
152 within the uterus, decidua, and cervix (Figure 2B-D and Supplementary file 1). A notable
153 increase in the Monocyte and Neutrophil populations was observed in the uterus and decidua
154 with preterm labor, with the NK cell-2 and Plasmocyte subsets also showing changes (Figure
155 2B&C). Moreover, Dendritic cells were increased in the decidua (Figure 2C), with a similar
156 tendency observed in the uterus (Figure 2B). Interestingly, the Macrophage-1 cell type was
157 decreased in the uterus with preterm labor (Figure 2B). Although not visually apparent from the
158 UMAP plots, both the uterus and decidua showed a substantial decrease in non-immune subsets
159 such as Fibroblast-1, -2, and Stromal-3 with preterm labor (Figure 2B&C), with Stromal-2 also
160 showing modest changes in the uterus (Figure 2B). In contrast with these two tissues, the cervix

161 only showed changes in two cell types: Neutrophil and Epithelial-8 were both increased with
162 preterm labor (Figure 2D), indicating that a modest cellular response to intra-amniotic infection
163 does occur in this tissue.

164 To validate the leukocyte infiltration observed in the reproductive tissues, we performed
165 immunohistochemistry staining to detect leukocytes using the pan-marker CD45, followed by the
166 identification of major immune cell subsets using multiplex immunofluorescence (Figure 2E-G).
167 Consistent with the cell abundances derived from scRNA-seq, leukocyte infiltration was highly
168 evident in the uterus and decidua with preterm labor; uterine leukocytes were more evenly
169 distributed among neutrophils, monocytes, and macrophages, whereas decidual leukocytes were
170 predominantly neutrophils and, to a lesser extent, monocytes (Figure 2E&F). The degree of
171 leukocyte infiltration observed in the uterus and decidua with preterm labor was not evident in
172 control tissues (Figure 2-figure supplement 1D&E), given that these mice were not undergoing
173 labor. Similar to the scRNA-seq results, the leukocyte abundance in the cervical tissues was
174 largely comparable between the control and preterm labor groups (Figure 2G-figure supplement
175 1F).

176 Taken together, these findings highlight the distinct cellular composition of the uterus,
177 decidua, and cervix, and indicate that preterm labor resulting from intra-amniotic infection
178 involves changes in both the immune and non-immune cellular repertoire of these tissues.

179

180 **Preterm labor induced by *E. coli* dysregulates gene expression within immune and non-**
181 **immune cell types in the reproductive tissues**

182 Given that preterm labor altered the cellular composition of the uterus, decidua, and
183 cervix, we next explored whether this inflammatory process also resulted in transcriptomic

184 changes to the identified cell types. Consistent with their altered abundance, multiple fibroblast,
185 stromal, and epithelial cell types in the uterus and decidua displayed upregulated gene expression
186 with preterm labor (Figure 3A&B and Supplementary file 2-3), while the cervical non-immune
187 cells with upregulated gene expression were exclusively epithelial (Figure 3C and
188 Supplementary file 4). Interestingly, innate immune cell types showed strong dysregulation of
189 gene expression in both directions that was inconsistent among tissues: while Monocyte showed
190 more downregulated differentially expressed genes (DEGs) in the uterus (Figure 3A) and cervix
191 (Figure 3C), this cell type showed more upregulated DEGs in the decidua (Figure 3B).
192 Neutrophil showed stronger downregulation of DEGs in the uterus and decidua (Figure 3A&B),
193 whereas in the cervix DEGs were primarily upregulated in this cell type (Figure 3C).
194 Macrophage-1, Dendritic cell, and NK cell-1 consistently displayed predominantly upregulated
195 DEGs in the uterus and decidua (Figure 3A&B), and were not represented in the cervix as
196 previously noted. In addition, the uterine Macrophage-2 and NK cell-2 populations displayed
197 upregulated DEGs (Figure 3A), which was not observed in other tissues (Figure 3B&C).
198 Although not as abundant as innate immune cells, the T cell population also displayed
199 upregulated DEGs with preterm labor in the uterus and decidua (Figure 3A&B). Thus, preterm
200 labor primarily induces gene expression in the dominant cell types from each tissue; yet, the
201 substantial amount of downregulated gene expression in innate immune cells may indicate a
202 switch from one transcriptomic program to another to better respond to infection.

203 We then utilized the Kyoto Encyclopedia of Genes and Genomes database to evaluate the
204 pathways enriched in preterm labor-associated DEGs in each cell type and thereby infer
205 functionality (Figure 3D). Strikingly, both immune and non-immune cell types with altered gene
206 expression in preterm labor showed enrichment of immunological pathways such as "cytokine-

207 cytokine receptor interaction", "NOD-like receptor signaling pathway", and "viral protein
208 interaction with cytokine and its receptor" across the three tissues (Figure 3D). Such findings are
209 consistent with previous studies showing the upregulation of immune-related pathways in
210 decidual endothelial [104] and stromal cells [70] from women with labor. Additional
211 inflammatory pathways such as "NK-kappa B signaling pathway" and "Toll-like receptor
212 signaling pathway" were also represented, to a lesser extent, by immune cells (e.g., NK cells and
213 Neutrophil) as well as non-immune cells such as epithelial cells, including in the cervix (Figure
214 3D). Together with the observed increase in cervical Epithelial-8 cell counts with preterm labor,
215 it is possible that the upregulation of inflammatory gene expression represents an infection-
216 induced differentiation of cervical epithelial cells to better participate in host defense
217 mechanisms in this compartment. Yet, while prior studies have indicated that the loss of cervical
218 epithelial integrity or function can increase susceptibility to ascending infection [105, 106], the
219 inverse relationship showing how intra-amniotic infection affects cervical cell composition
220 remains to be investigated.

221 The above data demonstrate that both immune and non-immune cell types in the
222 reproductive tissues display altered transcriptomic profiles with preterm labor that are primarily
223 characterized by upregulated gene expression. Yet, there is an overall tendency for the
224 enrichment of similar immunological pathways in both immune and non-immune cell types
225 across tissues, likely as part of the host response to intra-amniotic infection.

226

227 **Preterm labor induced by *E. coli* involves conserved cell types that display distinct**
228 **processes in the reproductive tissues**

229 The transcriptomic profiling of cell types suggested that specific subsets show conserved
230 responses with preterm labor across the reproductive tissues. Therefore, we next focused on the
231 shared preterm labor-specific gene expression among the uterus, decidua, and cervix. The Venn
232 diagram displayed in Figure 4A highlights the overlap in DEGs across tissues, particularly the
233 uterus and decidua. Correlation analyses indicated stronger relationships between preterm labor
234 and gene expression changes in the uterus and decidua than in the cervix (Figure 4B), which was
235 reflective of the total preterm labor-associated DEGs in each tissue. This observation was further
236 confirmed by the correlation between the gene expression profiles of the uterus and decidua,
237 which was stronger than the correlations between the decidua and cervix or the uterus and cervix
238 (Figure 4C). Given that the uterus, decidua, and cervix all displayed some degree of correlation
239 for preterm labor-associated gene expression, we evaluated the cell type-specific transcriptomic
240 changes that were conserved across all three tissues. We found that innate immune cell types
241 (Monocyte and Neutrophil) as well as non-immune cell types (Epithelial-3, -4, -6 and
242 Endothelial) showed conserved gene expression changes associated with preterm labor across the
243 uterus, decidua, and cervix (Figure 4D). We reasoned that, although the transcriptome profiles of
244 specific cell types were affected across all tissues, such cells may display distinct biological
245 processes according to their location. Gene Ontology (GO) analysis of the Neutrophil cell type in
246 the uterus, decidua, and cervix revealed that, while these cells shared some processes such as
247 "response to bacterium" and "response to lipopolysaccharide", processes specific to Neutrophils
248 in each tissue were also observed (Figure 4E). Uterine Neutrophils showed enrichment of
249 processes related to cytokine signaling and anti-viral response, whereas decidual Neutrophils
250 showed enrichment of cellular activation-associated processes (Figure 4E). In the cervix, unique
251 enriched Neutrophil processes were primarily associated with response to external stimuli and

252 bacteria (Figure 4E). Uterine and decidual Monocyte and Macrophage-1 cells also shared
253 enriched processes related to cytokine production and response to bacteria/lipopolysaccharide,
254 with decidual Monocytes also showing enrichment of activation-associated processes (Figure
255 4F). By contrast, cervical Monocytes displayed highly distinct processes related to protein
256 synthesis and humoral immune response (Figure 4F), suggesting that such cells may functionally
257 differ from their counterparts in the uterus and decidua. Epithelial-6, which had sufficient DEGs
258 to perform GO analysis in all three tissues, displayed largely consistent processes across the
259 uterus, decidua, and cervix that were related to inflammation, anti-bacterial response, and
260 cytokine production (Figure 4G). The uterine Epithelial-4 cell type displayed enrichment of
261 several chemotaxis-associated processes, suggesting involvement in leukocyte recruitment to this
262 tissue, whereas the cervical Epithelial-4 showed enrichment of effector functions such as
263 production of NO, IL-1, and IFNγ (Figure 4G). Epithelial-3, which only displayed sufficient
264 DEGs for GO analysis in the cervix, showed enrichment of multiple processes related to
265 promotion of B-cell and antibody responses (Figure 4G). Thus, the conserved cell types affected
266 by preterm labor in the uterus, decidua, and cervix each display distinct enrichment of biological
267 processes, suggesting that similar cell types display tissue-specific functions in the context of
268 intra-amniotic infection leading to preterm labor.

269 Given the higher degree of similarity in cell type-composition between the uterus and
270 decidua (Figure 1), we further investigated the biological processes enriched in several non-
271 immune cell subsets that were conserved between these two tissues with preterm labor (Figure 4-
272 figure supplement 2). Interestingly, Stromal-1 and Stromal-2 in the uterus showed largely similar
273 enrichment of biological processes, as did the Stromal-1 and Stromal-2 cell types in the decidua
274 (Figure 4-figure supplement 2A). Yet, these cell types differed between tissues, given that the

275 decidual stromal cells were enriched for leukocyte migration and chemotaxis whereas the uterine
276 stromal cells showed enrichment for response to immune signaling (Figure 4-figure supplement
277 2A). The Fibroblast-1 and Stromal-3 cell types showed less diversity in their enriched processes
278 compared between the uterus and decidua, with the former being associated with host defense
279 against infection and the latter associated with immune activation, including adaptive immunity
280 (Figure 4-figure supplement 2B). Fibroblast-2 and Fibroblast-3 were also comparable between
281 the uterus and decidua; however, the decidual Fibroblast-3 showed more striking enrichment of
282 responses to microorganisms and cytokine signaling (Figure 4-figure supplement 2C). Finally,
283 the uterine and decidual Endothelial cell types displayed similar enrichment of processes related
284 to host defense, innate immunity, and cytokine signaling, with the decidual subset showing
285 modestly higher enrichment for processes related to neutrophil migration (Figure 4-figure
286 supplement 2D).

287 Taken together, these data indicate that the uterus, decidua, and cervix showed shared and
288 cell type-specific gene dysregulation with preterm labor, with a larger overlap between uterine
289 and decidual cell types. Yet, similar cell types displayed distinct tissue-specific gene expression
290 profiles, pointing to differing functional roles for these cells in the host response to intra-
291 amniotic infection leading to preterm labor.

292

293 **Preterm labor influences cell-cell communications in the reproductive tissues**

294 Having established that preterm labor drives distinct transcriptomic changes in specific
295 cell types in the uterus, decidua, and cervix, we next leveraged our single-cell data to elucidate
296 cell-cell communication networks in these tissues.

297

Cell-cell communications in the uterus

The uterus is a highly heterogeneous organ with multiple described regions that differ in cellular composition and function [107-116]. To unravel the intercellular communications taking place in the murine uterus with preterm labor, we performed a correlation analysis across preterm labor-associated genes for each pair of identified cell types (Figure 5-figure supplement 3A). The strongest correlations were observed for non-immune cell types, such as stromal, epithelial, fibroblast, smooth muscle, and Endothelial cell types (Figure 5-figure supplement 3A), suggesting that these cells exhibit similar changes in gene expression with preterm labor. Innate and adaptive immune cell types also showed moderate correlations; namely, T cell, NK-cell-1, NK-cell-2, Macrophage-1, Macrophage-2, Monocyte, and Dendritic cell (Figure 5-figure supplement 3A). The cell types with the weakest correlations were primarily epithelial subsets as well as Neutrophil, Erythroid, Stromal-3, and SMC-2 (Figure 5-figure supplement 3A), indicating that such cells show more distinct gene expression changes with preterm labor.

We next used CellChat to infer cell-cell communications within the uterus using our single-cell gene expression data and a database of established interactions between signaling ligands, receptors, and their cofactors [117]. Signaling pathways that were enriched or diminished in preterm labor, as well as those that were unaffected by this process, are shown in Figure 5-figure supplement 3B and Supplementary file 5. The alluvial plots shown in Figure 5A&B display the major cell-cell communication processes taking place in the uterus as well as the cell types that participate as senders or receivers in each process. Both innate and adaptive immune cell subsets (Neutrophil, Macrophage-1, Monocyte, Dendritic cell, NK cell, T-cell) contribute to the top signaling pathways implicated in preterm labor, such as CCL, CXCL, complement, IFN-I, IL-1, and IL-6 (Figure 5A). Notably, multiple non-immune subsets also

321 participate in these processes; namely, fibroblast, stromal, epithelial, SMC, and Endothelial cell
322 types (Figure 5A). While both immune and non-immune cell types served as receivers of preterm
323 labor-associated signaling, specific responders to each pathway could be distinguished (Figure
324 5B). For example, the signaling pathway of IL-6, which is commonly utilized as a biomarker of
325 intra-amniotic inflammation [47], was primarily driven by immune cell types (Figure 5A); yet,
326 the receiver cells for this pathway were non-immune subsets (Figure 5B). Conversely, the
327 primary senders for the Annexin signaling pathway were non-immune cell types (Figure 5A),
328 with the downstream receivers being predominantly immune cells (Figure 5B). The changes in
329 cell-cell communication occurring as a result of preterm labor were visualized using the arrow
330 plot in Figure 5C, where the directionality of each cell type arrow reflects the propensity for
331 increased outgoing and/or incoming interaction strength. Cell types such as Macrophage-2,
332 Stromal-2, Stromal-3, and Fibroblast-3 showed primarily even increases in incoming and
333 outgoing signaling with preterm labor (Figure 5C). Other cell types were more biased towards
334 increased incoming interactions, such as Macrophage-1, Neutrophil, Dendritic cell, Plasmocyte,
335 Monocyte, and Epithelial-6, or outgoing interactions, such as Stromal-1, Fibroblast-1, and
336 Fibroblast-2 (Figure 5C). Interestingly, several cell types showed a net decrease in signaling with
337 preterm labor; namely, T cell and SMC-1 (Figure 5C).

338 The top 25% of aggregated cellular interactions in the uterus were then contrasted
339 between the control and preterm labor groups, emphasizing the overall increase in cell-cell
340 signaling with preterm labor as well as the incorporation of new signaling pathways from cell
341 types that were rarely present in control tissues, such as Neutrophil (Figure 5D). The overall
342 change in uterine cell signaling with preterm labor was generated for each cell type, illustrating
343 that specific subsets such as Endothelial and Macrophage-2 show overall reduced cell-cell

communication relative to the control tissue environment while others such as stromal cell types and Macrophage-1 have increased signaling (Figure 5E). We then generated circle plots of the major cell-cell signaling pathways identified in the uterus with preterm labor to unravel the top cellular contributors to each (Figure 5F). Similar to Figure 5D, a cut-off was used to display only the top 25% of predicted interactions for each pathway, as opposed to the complete senders and receivers displayed in the alluvial plots. As expected, inflammatory pathways such as IL-1 and IL-6 were only modestly represented or completely absent, respectively, in the control uterus and were noticeably increased with preterm labor (Figure 5F), which is consistent with the upregulated expression of these cytokines in the human and murine myometrium during preterm or term labor [118-121]. The top contributors to these pathways were innate immune cell types such as Neutrophil and Monocyte, with non-immune subsets such as Fibroblast-3 contributing to a lesser extent (Figure 5F). Other signaling pathways (e.g., CXCL, CCL, and Complement) were also predominantly driven by specific immune cell types, such as Neutrophil and Macrophage-1, whereas IFN-I was primarily derived from Epithelial-6 (Figure 5F).

Taken together, these findings highlight the complex cell-cell communication network taking place in the murine uterus and how such interactions are modulated by the inflammatory process of preterm labor in both immune and non-immune cell types.

Cell-cell communication in the decidua

We first examined the correlations across preterm labor-associated changes in gene expression for each pair of cell types identified in the decidua (Figure 6-figure supplement 4A). Similar to the uterine tissues, the strongest correlations were observed for non-immune cell types (e.g., stromal, epithelial, fibroblast, smooth muscle, and Endothelial), followed by innate and

367 adaptive immune cells, of which the macrophage and Monocyte clusters were best correlated
368 (Figure 6-figure supplement 4A). Similarly, the weakest correlations were observed for some
369 epithelial cell types and Neutrophils (Figure 6-figure supplement 4A). Thus, decidual cells
370 display preterm labor-associated changes in gene expression with varying magnitude of sharing
371 among cell types, which resemble those observed in the uterine tissues.

372 The inferred cell-cell signaling pathways that were enriched or diminished in the decidua
373 with preterm labor are shown in Figure 6-figure supplement 4B and Supplementary file 6. From
374 among these, the top pathways are displayed with their participating sender and receiver cell
375 types in Figure 6A&B. Similar to the uterine tissues, key cell-cell communication pathways were
376 primarily related to immune functions such as cytokine and chemokine signaling (Figure
377 6A&B). Unique among the three compared tissues, the IL-17 pathway was most prominent in the
378 decidua (Figure 6A&B), which was consistent with a previous report of IL-17 signaling in
379 endothelial cells derived from the human peripartum decidua [104]. Both immune and non-
380 immune cell subsets contributed as senders or receivers in these signaling pathways, including
381 the NK-cell-2 subset that was not implicated in uterine cell-cell signaling (Figure 6A&B). The
382 decidual Epithelial-5 cell type appeared to be primarily functioning as a receiver of cell-cell
383 signaling in this tissue (Figure 6A&B). We then visualized the preterm labor-driven changes in
384 incoming and outgoing signaling, and observed that subsets such as Monocyte, Macrophage-1,
385 Neutrophil, NK cells, and Dendritic cells showed predominantly increased incoming interactions
386 (Figure 6C). On the other hand, stromal and fibroblast subsets as well as T cells tended towards
387 increased outgoing signaling, while SMC-1 and Endothelial cells showed an overall reduction in
388 interaction strength (Figure 6C). Interestingly, outgoing interaction strength was greater in
389 decidual T cells compared to uterine T cells (Figure 6C vs. Figure 5C), which is consistent with

390 our prior studies indicating a role for T cell-derived signals in the pathophysiology of preterm
391 labor associated with intra-amniotic infection [122].

392 Consistent with enhanced cell-cell signaling in preterm labor, aggregated cellular
393 interaction plots demonstrated an overall net increase in decidual intercellular interactions
394 compared to controls (Figure 6D). This was reflected by the upregulated signaling observed in
395 the majority of cell types as represented in Figure 6E, of which the strongest differential increase
396 in interaction was observed in Monocytes. We then dissected the aggregated cell-cell interactions
397 according to the top pathways (Figure 6-figure supplement 4B), and noted that inflammatory
398 pathways such as IL-1, IL-6, and the decidua-specific IL-17 were primarily represented by the
399 preterm labor group (Figure 6F). The top contributors to IL-1 signaling in preterm labor were the
400 Macrophage-1, Neutrophil, Dendritic cell, Monocyte, and NK-cell-2 subsets, while IL-6
401 signaling appeared to be driven by only the latter two cell types (Figure 6F). Notably, the top
402 contributor to the decidual IL-17 signaling was T cell, potentially indicating the participation of
403 decidual Th17 cells in the inflammatory process of preterm labor (Figure 6F). This concept is
404 supported by prior research that reported higher concentrations of IL-17 in amniotic fluid from
405 women who delivered preterm with acute histological chorioamnionitis compared to those who
406 delivered at term, and the cellular source of this cytokine was shown to be T cells in the
407 chorioamniotic membranes of women with acute histologic chorioamnionitis [123]. More
408 recently, we demonstrated that decidual T cells expressing IL-22, a pleiotropic cytokine with
409 pro- and anti-inflammatory properties, are enriched in women who underwent preterm labor and
410 birth [122]. Together with our current findings, these data indicate that decidual T cells
411 participate in the local inflammatory response to intra-amniotic infection.

These data provide insight into the distinct cellular interactions taking place in the decidua during the process of preterm labor, including the involvement of cell types and signaling pathways not observed in other tissues. Yet, the decidua and uterus also share cell type-specific communications that are affected by preterm labor. It is worth mentioning that, given the close relationship between the decidua and placenta, it is likely that the cellular signaling processes taking place in the decidua do not represent a closed system but may also include outgoing and incoming signals involving placental cell types. This concept is supported by a prior study of the first trimester decidua and placenta that investigated the expression levels of ligand-receptor pairs and proposed that decidual tissue cells such as fibroblasts may communicate with placental trophoblast cell types [68]. Future investigations may further elucidate inter-tissue cellular signaling between the uterus, decidua, and placenta, and how such processes are implicated in preterm labor.

Cell-cell communication in the cervix

Our investigation of the cell type-specific changes taking place in the cervix with preterm labor had indicated that the Neutrophil and Monocyte subsets were most affected, in tandem with previous studies showing labor-associated infiltration of immune cells [92, 93, 124-126], as well as multiple epithelial cell subsets (Figures 2 and 3). Consistently, correlation analysis of these cell types showed that the strongest associations in gene expression changes driven by preterm labor were observed among epithelial cell types (Figure 7-figure supplement 5A), while Neutrophils and Monocytes showed modest correlation of genes affected by preterm labor (Figure 7-figure supplement 5A). Inferred cell-cell signaling pathways were noticeably fewer compared to the other tissues and included multiple processes unique to the cervix (Figure 7-

435 figure supplement 5B and Supplementary file 7), which could be attributed to the less diverse
436 cell type composition observed in this tissue. Indeed, as shown by the participating senders and
437 receivers, signaling pathways that were strongly implicated in the uterus and decidua with
438 preterm labor were not as enriched in cervical cell types (Figure 7A&B). On the other hand, cell-
439 cell signaling pathways related to extracellular matrix were strongly represented (Figure 7A&B),
440 which is consistent with the primarily connective tissue composition of the cervix [127-129]. As
441 expected, given their inferred roles as receivers, most cervical epithelial cell types showed strong
442 incoming interactions with preterm labor, whereas the SMC-1, Fibroblast-2, and Stromal-1
443 subsets showed a tendency towards increased outgoing interactions (Figure 7A, C). This was
444 further supported by the aggregated cervical cell-cell interactions in the control and preterm
445 labor groups showing increased receipt of signaling by Epithelial-1 and Epithelial-8 (Figure 7D).
446 The overall differential interactions were consistent with the predominant role of SMC-1 and
447 Fibroblast-2 as senders of cell-cell signaling and epithelial subsets as receivers (Figure 7E). A
448 previous histological investigation of cervical biopsies from intrapartum and non-pregnant
449 women indicated a pregnancy-specific accumulation of myofibroblast cells, which could be
450 interacting with the extracellular matrix to aid in supporting the mechanical stresses present
451 during labor [130]. Histologically, such myofibroblasts displayed features of both fibroblast and
452 smooth muscle cells [130]; yet, it was also noted that myofibroblasts were less abundant and
453 spatially restricted in rat cervical tissues compared to the human cervix [131], Furthermore, in
454 the last decade, a new paradigm for the role of SMCs in the human cervix has emerged,
455 suggesting a sphincter-like function of the internal os, in which the SMCs express contractility-
456 associated proteins that are responsive to oxytocin signaling [132]. Therefore, these studies
457 support the observed involvement of SMC-1 and Fibroblast-2 subsets in preterm labor-associated

458 signaling in the murine cervix herein. We then dissected the individual signaling pathways
459 driven by cervical cell types, and noted that the most obvious change driven by preterm labor
460 was observed for the IL-1 signaling pathway in which Epithelial-2 was the top participant
461 (Figure 7F), supporting the role of IL-1 as a mediator of parturition [133-136].

462 Together, these findings further emphasize the unique cell-cell signaling pathways taking
463 place in the cervix during preterm labor, which are primarily driven by the non-immune cells in
464 this compartment.

465

466 **Comparison of the uterine transcriptomic effects of preterm labor induced by local or**
467 **systemic inflammation**

468 Preterm labor is associated with intra-amniotic infection that is frequently subclinical
469 (i.e., occurring in the absence of maternal symptoms) [4, 83, 137-139]. This clinical scenario has
470 been most closely replicated using murine models of the intra-amniotic injection of bacteria [77,
471 122] or their products [76, 140, 141], as we have previously demonstrated. However, a subset of
472 spontaneous preterm labor cases occurs in the clinical setting of a maternal systemic
473 inflammatory response, such as pyelonephritis [142-147]. In a previous study, we utilized two
474 models of preterm birth induced by intra-amniotic or systemic maternal inflammation and
475 evaluated the resulting inflammatory response in the mother and fetus [141]. Both intra-amniotic
476 and systemic maternal inflammation resulted in preterm birth [141], which led us to propose that
477 these inflammatory processes may induce overlapping transcriptomic changes in the uterine
478 tissues. Therefore, we compared the current uterine scRNA-seq data to a uterine bulk
479 transcriptomic dataset derived from mice that underwent preterm labor induced by systemic
480 maternal inflammation [62] (Figure 8A). To compare these datasets, cell type-assignment of

481 uterine scRNA-seq-derived DEGs was ignored, thereby obtaining a pooled "pseudobulk" dataset
482 that was directly compared to the previously generated uterine bulk transcriptomic dataset.
483 Correlation analysis of the DEGs from uterine pseudobulk data and bulk transcriptomic data
484 indicated a high degree of shared changes in gene expression with preterm labor induced by
485 intra-amniotic or systemic inflammation (Figure 8B). Each dataset also contained preterm labor-
486 associated DEGs that were not identified in the other dataset (Figure 8B); yet, whether such
487 unique DEGs are driven more by inherent differences between scRNA-seq and bulk tissue
488 sequencing technologies, or by differences in the uterine response to intra-amniotic vs. systemic
489 inflammation, cannot be ascertained here. To infer cell type-specific changes in gene expression
490 within the bulk dataset, we used the annotated expression profiles of each cell type identified by
491 scRNA-seq and overlaid these with the bulk data. Correlation analysis was then performed to
492 evaluate whether changes in cell type-specific gene expression were correlated in magnitude and
493 direction between the scRNA-seq and bulk datasets (Figure 8C). Notably, significant agreement
494 was observed for the majority of cell type-specific gene expression changes between the datasets
495 (Figure 8C). The DEGs assigned to the Epithelial-4 and SMC-2 cell types showed only slight
496 agreement between scRNA-seq and bulk datasets (Figure 8C); for the latter subset, this could
497 potentially be explained by the limited capacity of the 10x Genomics technology to encapsulate
498 smooth muscle cells above a specific size threshold, as we have previously reported [71].
499 Nonetheless, these data indicate a substantial degree of overlap between the uterine gene
500 expression changes associated with intra-amniotic inflammation or systemic maternal
501 inflammation leading to preterm labor and birth.
502

503 **Shared cellular signaling pathways in the murine uterus and human myometrium during**
504 **the processes of preterm and term labor**

505 Lastly, to examine the cell types that contribute to the process of labor in mice and
506 humans, we utilized the differential cellular interactions in the murine uterus with preterm labor
507 together with our previously generated single-cell atlas of the human myometrium with labor at
508 term [71] (Figure 9). We investigated the interaction strength between cell types affected by
509 labor as well as prominent signaling pathways, and contrasted these between the murine and
510 human tissues. Overall, we found that labor-associated cell-cell interactions were primarily
511 driven by SMC, stromal, fibroblast, and innate immune cell types in both the murine uterus and
512 human myometrium, independent of differences in sender/receiver status (Figure 9A&B).

513 Specifically, in the murine uterus, non-immune cell types such as Fibroblast-1, -2, and -3,
514 Stromal-2 and -3, and SMC-1 showed the strongest labor-associated increase in outgoing cell-
515 cell signaling, whereas outgoing signaling by Macrophage-2 was greatly diminished (Figure 9A).
516 The top receivers of labor-associated signaling were Fibroblast-3, Stromal-2 and -3, and
517 Epithelial-6 as well as innate immune cell types (Monocyte, Neutrophil, and Macrophage-1)
518 (Figure 9A). Endothelial, SMC-1, Plasmocyte, and Macrophage-2 showed diminished incoming
519 signaling with preterm labor (Figure 9A).

520 In the human myometrium, labor involved increased outgoing signaling almost
521 exclusively by smooth muscle cell and stromal subsets, with Myofibroblast and LED cells also
522 contributing to this process (Figure 9B). Receivers of such outgoing interactions included
523 macrophage subsets and Monocytes, which is consistent with previous investigations indicating
524 that myometrial cell contraction during labor is promoted by crosstalk with macrophages in a co-
525 culture model [148]. Multiple myometrial cell subsets displayed substantially reduced outgoing

526 signaling with labor, such as EVT, Macrophage-4, Plasmablast, Unciliated Epithelial, and ILC
527 (Figure 9B). For incoming signaling, the majority of human myometrial cell types tended to have
528 increased interaction only with those cells that displayed greater outgoing signals, such as
529 smooth muscle and stromal cells (Figure 9B). Some exceptions seemed to be the Macrophage-1,
530 SMC-3, and Stromal-1 subsets, whose incoming signaling from the majority of other cell types
531 was strengthened (Figure 9B).

532 We then examined the top 25% of aggregated cell-cell interactions in the human
533 myometrium at term without labor and at term with labor (Figure 8B-figure supplement 6A).
534 Consistent with the correlation analysis above (Figure 9B), a clear shift in the cell types
535 contributing to myometrial cell-cell signaling was observed between groups, with the EVT,
536 Macrophage-4, Plasmablast, and Unciliated epithelial clusters showing greatly diminished
537 interactions in labor, and smooth muscle and stromal cell subsets acquiring increased interactions
538 (Figure 8B-figure supplement 6A). This shift in interaction with labor was also reflected by the
539 combined differential interaction analysis shown in Figure 8B-figure supplement 6B. When
540 examining the specific cell-cell signaling pathways that were impacted by labor, terms such as
541 Collagen, IL-1, CCL, Complement, and CXCL were found to be shared between the murine
542 uterus and human myometrium, indicating shared labor-associated cellular signaling between
543 species (Figure 8D-figure supplement 6C); yet, the closer inspection of these shared signaling
544 pathways revealed differences in the cell types contributing to each (Figure 9C&D). The
545 relevance of immune pathways such as chemokine signaling in the process of labor is supported
546 by previous reports demonstrating that the use of a chemokine inhibitor on human myometrial
547 cells decreased contraction and gap junction formation, thereby disrupting intercellular
548 communication [149, 150]. Taken together, these data indicate that labor-associated cell-cell

549 interactions heavily involve SMC, stromal, fibroblast, and innate immune cell types in the
550 murine uterus and the human myometrium, providing evidence of labor-specific signaling
551 processes between immune and non-immune cells that are shared between species.
552

553 **Conclusion**

554 In summary, the current study provides a single-cell atlas of the murine uterus, decidua,
555 and cervix and highlights the shared and distinct patterns of cell type composition, transcriptional
556 profiles, and cell-cell signaling among these tissues induced by intra-amniotic infection leading
557 to preterm labor and birth. scRNA-seq revealed that preterm labor affects the cellularity of the
558 uterus, decidua, and cervix not only through the infiltration of innate immune cells but also
559 through the altered transcriptomic profiles of non-immune cell types. Importantly, gene
560 expression analysis indicated shared modulation of uterine and decidual cell types, with the
561 cervix showing more distinct changes. Yet, affected cell types showed distinct host immune
562 responses according to location, indicating tissue-specific functions of these cells. Cell-cell
563 communication analysis indicated the participation of immune and non-immune cell types in
564 multiple inflammatory signaling pathways associated with preterm labor in the uterus, decidua,
565 and cervix. Correlation analysis of uterine scRNA-seq or bulk transcriptomic data from mice
566 with local or systemic inflammation-induced preterm labor, respectively, indicated a substantial
567 overlap in labor-associated gene expression changes. Lastly, comparison of cell-cell
568 communication in the murine uterus with preterm labor and the human myometrium with term
569 labor revealed shared cell types and signaling pathways implicated in the process of parturition.
570 Together, our findings provide novel insight into the cellular changes taking place in the murine
571 reproductive tissues during preterm labor leading to premature birth.

MATERIALS AND METHODS

Mice

Mice were purchased from The Jackson Laboratory (Bar Harbor, ME, USA) and bred in the animal care facility at the C.S. Mott Center for Human Growth and Development, Wayne State University (Detroit, MI, USA). Mice were under a circadian cycle of light:dark = 12:12 h. Eight- to twelve-week-old C57BL/6 (RRID:IMSR_JAX:000664) female mice were bred with BALB/cByJ male mice (RRID:IMSR_JAX:001026), and females were examined daily between 0800 and 0900 to check for the presence of a vaginal plug, which was considered as 0.5 days *post coitum* (dpc). Upon observation of a vaginal plug, females were removed from mating cages and housed separately, and their weights were monitored daily. At 12.5 dpc, a weight gain of ≥2g was considered confirmation of pregnancy. Mice were randomized to receive intra-amniotic injection of *E. coli* or vehicle control, and investigators were not blinded to control or treatment assignment. No experimental mice were excluded from analysis. All procedures and experiments were approved by the Institutional Animal Care and Use Committee (IACUC) at Wayne State University under Protocol nos. 18-03-0584 and 21-04-3506.

Preparation of E. coli culture for intra-amniotic injection

Escherichia coli was purchased from the American Type Culture Collection (ATCC, Manassas, VA, USA) (ATCC 12014) and was grown in Luria-Bertani (LB) broth (cat. no. L8050, Teknova, Hollister, CA, USA) at 37°C. From an overnight culture, a sub-culture was placed with fresh LB broth and grown to the logarithmic phase (OD_{600} 0.9 - 1). Additional dilution was performed using sterile 1X phosphate-buffered saline (PBS, Thermo Fisher Scientific/Gibco, Grand Island, NY, USA) to reach a working concentration of 10 CFU/25µL.

Measurement of cervical length by ultrasound

Dams were anesthetized on 16.5 dpc by inhalation of 2% isoflurane (Aerrane; Baxter Healthcare Corporation, Deerfield, IL, USA) and 1 to 2 liters/min of oxygen in an induction chamber. Anesthesia was maintained with a mixture of 1.5 to 2% isoflurane and 1.5 to 2 liters/min of oxygen. Mice were positioned on a heating pad and stabilized with adhesive tape. Fur removal from the abdomen was performed using Nair cream (Church & Dwight Co., Inc., Ewing, NJ, USA). Sterile forceps were utilized to expose the vulva and 200 µL of Sterile Aquasonic® 100 ultrasound transmission gel (Parker laboratories, Fairfield, NJ, USA) was used to fill the vagina to create contrast and allow for clear visualization of the external limit of the uterine cervix (i.e., the external os). A trans-abdominal ultrasound approach was utilized to evaluate the cervix. The transducer was slowly moved toward the lower part of the abdomen and the cervix was positioned in a longitudinal view. The cervical length was measured from the internal to the external OS at least three times per mouse, and its average was utilized as the final value for cervical length. This procedure was performed prior to ultrasound-guided injection with either *E. coli* or PBS and repeated 24 h later (on 17.5 dpc) (i.e., prior to tissue collection).

Intra-amniotic inoculation with E. coli

Dams that underwent cervical measurement were maintained on the heating pad under anesthesia as described above. The ultrasound transducer was slowly moved toward the abdomen to localize the amniotic sacs. The syringe with *E. coli* suspension (10 CFU/25µL) was stabilized by a mechanical holder (VisualSonics). Ultrasound-guided intra-amniotic inoculation with *E. coli* was performed in each amniotic sac using a 30G needle (BD PrecisionGlide needle; Becton

Dickinson, Franklin Lakes, NJ, USA). Controls were injected with 25 µL of sterile 1X PBS into each amniotic sac. After the ultrasound injection, the dams were placed under a heat lamp for recovery (defined as when the mouse resumed normal activities such as walking and responding), which typically occurred 10 min after removal from anesthesia. After recovery, mice were video monitored to observe pregnancy outcomes.

Video Monitoring

Pregnancy outcomes were recorded via video camera (Sony Corporation, Tokyo, Japan) to determine gestational length, and therefore rate of preterm birth. Preterm birth was defined as delivery occurring before 18.5 dpc, and its rate was represented by the percentage of females delivering preterm among the total number of mice injected.

Tissue collection prior to preterm birth

Dams were euthanized on 17.5 dpc and the reproductive tissues (uterus, decidua, and cervix) were collected. Tissues collected for the preparation of single-cell suspensions were placed in sterile 1X PBS, while tissues for histological analyses were fixed in 10% Neutral Buffered Formalin (Surgipath, Leyca Biosystems, Wetzlar, Germany) and embedded in paraffin. Five-µm-thick sections were cut and mounted on Superfrost® Plus microscope slides (Cat. No. 48311-703, VWR International, LLC. Radnor, PA, USA).

Histological characterization of murine reproductive tissues

Leukocyte detection using DAB immunohistochemistry

Five-µm-thick tissue sections from mice injected with PBS or *E. coli* were deparaffinized and rehydrated using xylene and a series of decreasing ethanol concentrations, respectively. Immunohistochemistry staining using the Monoclonal Rabbit Anti-Mouse CD45 (AB_2799780; clone D3F8Q, cat. no. 70257S, Cell Signaling Technology, Danvers, MA, USA) was performed using the Leica Bond Max Automatic Staining System in a peroxidase-mediated oxidation of 3,30-diaminobenzidine (DAB) from the Bond™ Polymer Refine Detection Kit (both from Leica Microsystems, Wetzlar, Germany). The negative control used was the Rabbit FLEX Universal Negative Control (cat. no. IR60066-2, Agilent, Santa Clara, CA, USA). Images were scanned using the Brightfield setting of the Vectra Polaris Multispectral Imaging System.

Movat's pentachrome staining

Five-µm-thick tissue sections from mice injected with PBS or *E. coli* were histologically characterized for the presence of collagen, elastin, muscle, and mucin using the Movat Pentachrome Stain Kit (Modified Russell-Movat; ScyTek Laboratories, Inc. Logan, UT, USA), following manufacturer's instructions with modifications. Briefly, tissue sections were deparaffinized, stained with working Elastic Stain solution for 20 min, and rinsed in running tap water for 1 min followed by rinsing with deionized water. Then, the following reagents from the kit were sequentially applied to the entire tissue section with distilled water rinsing in between each application: 2% Ferric Chloride for 5-8 s, 5% Sodium Thiosulfate Solution for 1 min, Alcian Blue Solution (pH 2.5) for 20 min, Biebrich Scarlet-Acid Fuchsin Solution for 2 min, 5% Phosphotungstic Acid Solution for 7 min, and 1% Acetic Acid Solution for 3 min. Excess Acetic Acid Solution was drained from the slides and Yellow Stain Solution was immediately applied for 20 min. The slides were then rinsed in 100% ethanol followed by rinsing with xylene. Images

were scanned using the Brightfield setting of the Vectra Polaris Multispectral Imaging System (Akoya Biosciences, Marlborough, MA, USA).

OPAL multiplex immunofluorescence

OPAL multiplex immunofluorescence staining was performed using the OPAL Multiplex 7-color IHC kit (Cat. no. NEL811001KT; Akoya Biosciences), according to the manufacturer's instructions. Prior to multiplex staining, the order of antibody staining was optimized using single-plex staining paired with tyramide signal amplification (TSA)-conjugated OPAL fluorophores. The optimized detection panel includes antibody-OPAL fluorophore pairs in the following order: Monoclonal Rabbit Anti-Mouse F4/80 (AB_2799771; clone D2S9R; cat. no. 70076s, Cell Signaling Technology) with OPAL 520, Monoclonal Rabbit Anti-Mouse CD3ε (AB_2889902; clone E4T1B; cat. no. 78588s, Cell Signaling Technology) with OPAL 570, Monoclonal Rabbit Anti-Mouse Klrb1c/CD161c (AB_2892989; clone E6Y9G; cat. no. 39197S, Cell Signaling Technology) with OPAL 620, Polyclonal Rabbit Anti-Mouse Ly6C (cat. no. HA500088, HuaBio, Boston, MA, USA) with OPAL 650, and Monoclonal Rabbit Anti-Mouse Ly6G (AB_2909808; clone E6Z1T; cat. no. 87048S, Cell Signaling Technology) with OPAL 690. The Rabbit FLEX Universal Negative Control (Agilent) was used as isotype. Briefly, 5-µm-thick tissue sections from mice injected with PBS or *E. coli* were deparaffinized and rehydrated using xylene and a series of decreasing ethanol concentrations, respectively. The slides were rinsed in deionized water and epitope retrieval was performed by submerging the slides in appropriate antigen retrieval (AR) buffer and boiling in a microwave oven. Non-specific binding was prevented by incubating slides in OPAL antibody diluent/blocking solution prior to incubating with each primary antibody at room temperature. Next, the slides were rinsed in

TBST prior to incubation with anti-mouse secondary antibody-horse radish peroxidase (HRP) conjugate followed by the selected TSA-conjugated OPAL fluorophore. Cycles of sequential epitope retrieval, target detection, and signal amplification were repeated using the optimized antibody-OPAL fluorophore pair. Once all targets were detected, the slides were incubated with DAPI (4′,6-diamidino-2-phenylindole) as a nuclear counterstain and mounted using AquaSlip™ Aqueous Permanent Mounting Medium (American MasterTech). Fluorescence image acquisition was performed using the Vectra Polaris Multispectral Imaging System at 20x magnification. Multispectral images were analyzed using the inForm software version 2.4 (Akoya Biosciences).

Tissue dissociation of murine uterus and decidua

Immediately following tissue collection, the uterus and decidua were dissociated to prepare single-cell suspensions. The tissues were mechanically dissociated and enzymatically digested by incubating at 37ºC using enzymes from the Umbilical Cord Dissociation Kit (Miltenyi Biotec). A second round of mechanical dissociation was performed using the gentleMACS Dissociator (Miltenyi Biotec), and dissociated cells were rinsed with 1X PBS (Thermo Fisher Scientific) prior to filtration using a 100µm cell strainer (Miltenyi Biotec). Filtered cells were pelleted by centrifugation at 300 x g for 5 min, erythrocytes were eliminated using ACK Lysing Buffer (Life Technologies), and the cells were rinsed in 0.04% BSA (Sigma Aldrich) and 0.5 mM EDTA (Sigma Aldrich) diluted in 1X PBS. Finally, the cells were filtered using a 30µm cell strainer (Miltenyi Biotec), and the Dead Cell Removal Kit was used to remove dead cells to obtain a cell viability of ≥80%.

Tissue dissociation of the murine cervix

Immediately following the collection of the cervix, the tissue was mechanically dissociated and enzymatically digested using Collagenase A (160 mg/mL) (Sigma Aldrich, St. Louis, MO, USA) and incubated at 37ºC. Then, the dissociated cells were pelleted by centrifugation at 16,000 x g for 10 min at 20ºC and resuspended with 0.05% trypsin-EDTA (Thermo Fisher Scientific, Waltham, MA) prior to a second round of mincing and incubation in 0.05% trypsin-EDTA at 37ºC. The enzymatic reaction was stopped by the addition of FBS (Fetal Bovine Serum, Thermo Fisher). Cells were then filtered using a 70µm cell strainer (Miltenyi Biotec, San Diego, CA, USA) and pelleted by centrifugation at 300 x g for 10 min. Erythrocytes were removed using ACK Lysing Buffer (Life Technologies, Grand Island, NY, USA). Finally, the cells were resuspended in 0.04% Bovine Serum Albumin (BSA) (Sigma Aldrich) diluted in 1X PBS (Thermo Fisher Scientific, NY, USA) and filtered through a 30µm cell strainer (Miltenyi Biotec). The cell concentration and viability were determined using an automatic cell counter (Cellometer Auto 2000, Nexcelom Bioscience, Lawrence, MA, USA) and the Dead Cell Removal Kit (Miltenyi Biotec) was used to remove dead cells to obtain a cell viability of ≥80%.

Generation of gel beads-in-emulsion (GEMs) and library preparation

Generation of gel beads-in-emulsion (GEMs) and preparation of library constructs was performed on viable single-cell suspensions using the 10x Genomics Chromium Single Cell 3' Gene Expression Version 3.1 Kit (10x Genomics, Pleasanton, CA, USA), according to the manufacturer's instructions. Briefly, viable single cells were encapsulated in partitioning oil together with a single Gel Bead with barcoded oligonucleotides within the Chromium Controller. Reverse transcription of mRNA into complementary (c)DNA was performed using the Veriti 96-well Thermal Cycler (Thermo Fisher Scientific, Wilmington, DE, USA). Dynabeads MyOne

SILANE (10x Genomics) and the SPRIselect Reagent (Beckman Coulter, Indianapolis, IN, USA) were used to purify resulting cDNA, which was optimized by enzymatic fragmentation, end-repair, and A-tailing. Next, adaptors and sample index were incorporated by ligation. The sample index PCR product was then amplified using the Veriti 96-well Thermal Cycler and double-sided size selection was performed using the SPRIselect Reagent kit. Following the formation of cDNA and final library construct, the Agilent Bioanalyzer High Sensitivity DNA Chip (Agilent Technologies, Wilmington, DE, USA) was used determine sample quality and concentration.

Sequencing

Prior to sequencing of post-library constructs, samples were quantified using the Kapa DNA Quantification Kit for Illumina platforms (Kapa Biosystems, Wilmington, MA, USA), following the manufacturer's instructions. The sequencing of 10x scRNA-seq libraries was performed on the Illumina NextSeq 500 at the Genomics Services Center (GSC) of the Center for Molecular Medicine and Genetics (Wayne State University School of Medicine, Detroit, MI, USA). The Illumina 75 Cycle Sequencing Kit (Illumina, San Diego, CA, USA) was used with 58 cycles for R2, 26 for R1, and 8 for I1.

Data analysis

scRNA-seq data normalization and pre-processing

Sequencing data were processed using Cell Ranger version 4.0.0 (10x Genomics). The "cellranger counts" was also used to align the scRNA-seq reads by using the STAR aligner [151] to produce the bam files necessary for demultiplexing the individual of origin based on genotype

information using demuxlet [152] and a custom vcf file. The genotype data were downloaded from ftp://ftp-mouse.sanger.ac.uk/current_snps/mgp.v5.merged.snps_all.dbSNP142.vcf.gz, the strains C57BL_6NJ and BALB_cJ were extracted, and a new synthetic vcf file was generated consisting of all the genetic variants where these two strains diverge, and containing a maternal genotype column identical to the C57BL_6NJ strain and a fetal genotype column with a "0/1" heterozygote genotype. Ambient RNA contamination and doublets were removed using SoupX version 1.5.2 [153] and DoubletFinder 2.0.3 [154]. Additionally, any cell with < 200 genes or > 20,000 genes detected, or that had > 10% mitochondrial reads, was excluded. All count data matrices were then normalized and combined using the Seurat package in R (Seurat version 4.0.3) [155, 156]. The first 100 principal components were obtained, and the different libraries were integrated and harmonized using the Harmony package in R version 1.0.0 [157]. The top 30 harmony components were then processed to embed and visualize the cells in a two-dimensional map via the Uniform Manifold Approximation and Projection for Dimension Reduction (UMAP) algorithm [158, 159]. A resolution of 0.5 was used to cluster the single cells.

Annotation of cell types

The SingleR [160] package in R version 1.6.1 was used to annotate cell types based on their similarities to reference datasets with known labels [161, 162]. SingleR annotates single cells from query data by computing the Spearman's correlation coefficient between the single-cell gene expression data and samples from the reference dataset. The correlation is measured only based on the variable genes in the reference dataset. The multiple correlation coefficients per cell type are combined according to the cell type labels of the reference dataset to assign a score per cell type. Additionally, we confirmed the cell type identities by identifying the top

DEGs (see below) and the gene-cell type mapping data provided by the Mouse Cell Atlas and single-cell MCA (scMCA) package [163] in R version 0.2.0. Using different annotations obtained from the reference mapping workflows, the final cell type labels were assigned based on a majority vote. If multiple clusters were assigned to the same consensus cell type, we added a sub-index to that cell type for each different original Seurat cluster: Clusters 0, 1, and 21 were annotated as Fibroblast-1, Fibroblast-2, and Fibroblast-3; clusters 2, 4, and 12 were annotated as Stromal-1, Stromal-2 (Decidua), and Stromal-3; clusters 5, 7, 8, 10, 11, 13, 14, 20, 23, and 28 were annotated as Epithelial-1 (basal), Epithelial-2 (squamous), Epithelial-3 (squamous), Epithelial-4 (glandular), Epithelial-10 (proliferative), Epithelial-5 (luminal), Epithelial-6 (secretory), Epithelial-7 (glandular), Epithelial-8 (Enterocyte), and Epithelial-9 (Secretory); clusters 9 and 24 were annotated as Macrophage-1 and Macrophage-2 (progenitor); clusters 15 and 26 were annotated as SMC-1 and SMC-2; and clusters 19 and 27 were annotated as NK-cell-1 and NK-cell-2. All remaining clusters were assigned a unique cell type identifier.

Differential gene expression for cell type analysis

For this analysis, the differential expression of selected marker genes for each cell type/cluster was identified using the Wilcoxon Rank Sum test and the FindAllMarkers function from Seurat (see Supplementary file 8). For this analysis, we first compared each cluster to all cell types. We further used the top cell markers [ranked based on $\log_2$(Fold change) and requiring $q < 0.1$] assigned to each sub-cluster to annotate the clusters using the Mouse Cell Atlas and scMCA package [163].

Differential gene expression in preterm labor

The identification of preterm labor-associated DEGs between study groups was performed using the DESeq2 R package version 1.32.0 [164]. A term for each library was added to the DESeq2 model to correct for technical batch effects (library identifier). For each cell type/replicate combination, we only used combinations with more than 20 cells; otherwise, it was treated as non-observed. Cell types found in < 3 combinations per study group were dropped from the differential gene expression analysis (Supplementary file 9 contains all genes determined as differentially expressed).

Gene ontology and pathway enrichment analysis of genes affected by preterm labor

The clusterProfiler in R version 4.0.4 [165] was used to perform the Over-Representation Analysis (ORA) separately for each list of genes obtained as differentially expressed for each cell type based on the Gene Ontology (GO), Kyoto Encyclopedia of Gene and Genomes (KEGG), and Reactome databases. The functions "enrichPathway", "enrichKEGG", and "enrichGO", from "clusterProfiler" were used. In ORA analyses, the universe of genes for each cell type was the subset that was expressed at a level sufficient to be tested in differential gene expression analysis. When results are combined across cell types, any genes tested (with a calculated p-value) in any of the cell types are used for the universe. Only ORA results that were significant after correction were reported with $q < 0.05$ being considered statistically significant.

Cell-cell communication analysis

CellChat [117] was used to infer the cell-cell communications using the single-cell gene expression data from preterm labor and control conditions and a database of prior knowledge of the interactions between signaling ligands, receptors, and their cofactors. The top 25% of

824 significant cell-cell communications ($p < 0.05$) across different pathways were shown for the two
825 conditions of preterm labor and control. Next, the aggregated cell-cell communication between
826 different cell groups was calculated for the two study groups, and the interaction strength was
827 compared among different cell types from the two study groups. The differential interaction
828 strength was represented with circle plots with red (or blue) edges showing the increased (or
829 decreased) signaling in preterm labor compared to controls. Additionally, the detailed differential
830 interaction strengths were shown using heatmap representations. Major signaling sender and
831 receiver cells were displayed using scatter plots where the changes in signaling strength from
832 control to preterm labor were represented by arrows. The R packages CellChat version 1.1.2,
833 ggalluvial version 0.12.3, and ggplot2 version 3.3.5 were used to visualize cell-cell
834 communication analyses. The major sending and receiving signaling roles based on context-
835 specific pathways across different cell groups were identified using a cut-off of 0.5 when
836 visualizing the connection. The overall information flow [sum of the significant communication
837 probability ($p < 0.05$) in the inferred cell-cell network] for each signaling network was
838 represented using a bar plot. The comparison between the overall information flow from the two
839 study groups (preterm labor and control) was performed using the paired Wilcoxon test with the
840 function "rankNet" from CellChat.

841

842 *Comparison between murine uterine single-cell and bulk transcriptomic data*

843 The cell type-specific and pseudo-bulk preterm labor-associated DEGs were identified
844 using the DESeq2 R package and compared with the DEGs from the bulk uterine RNA
845 sequencing data from mice intra-peritoneally injected with LPS [62].

846

Comparison between cell-cell communication in human and murine uterine tissues

We inferred cell-cell communications using the human myometrial single-cell gene expression data from term in labor (TIL) and term without labor (TNL) study groups [71], and compared the inferred interactions between mouse (uterus) and human (myometrium) across the top common signaling pathways with highest numbers of DEGs.

Statistics

Observational mouse data were analyzed by using SPSS v19.0 and GraphPad Prism version 8. For comparing the rates of preterm birth, the Fisher's exact test was used. For gestational length and cervical length, the statistical significance of group comparisons was assessed using the Mann-Whitney U-test or paired t-test, respectively.

Data and materials availability

The scRNA-seq data reported in this study has been submitted to the Gene Expression Omnibus repository (GEO accession number GSE200289). All software and R packages used herein are detailed in materials and methods section. Scripts detailing the single-cell analysis are available at GitHub (https://github.com/piquelab/murine_scRNA).

ACKNOWLEDGEMENTS

Figures include art created with BioRender.com

COMPETING INTERESTS

The authors declare that no competing interests exist.

FUNDING

This research was supported, in part, by the Perinatology Research Branch, Division of Obstetrics and Maternal-Fetal Medicine, Division of Intramural Research, *Eunice Kennedy Shriver* National Institute of Child Health and Human Development, National Institutes of Health, U.S. Department of Health and Human Services (NICHD/NIH/DHHS); and, in part, with Federal funds from NICHD/NIH/DHHS under Contract No. HHSN275201300006C. Dr. Romero has contributed to this work as part of his official duties as an employee of the United States Federal Government. This research was also supported by the Wayne State University Perinatal Initiative in Maternal, Perinatal and Child Health. The funders had no role in the study design, data collection and analysis, decision to publish, or preparation of the manuscript.

REFERENCES

1. Liu, L., et al., *Global, regional, and national causes of child mortality in 2000-13, with projections to inform post-2015 priorities: an updated systematic analysis.* Lancet, 2015. **385**(9966): p. 430-40.
2. Chawanpaiboon, S., et al., *Global, regional, and national estimates of levels of preterm birth in 2014: a systematic review and modelling analysis.* Lancet Glob Health, 2019. **7**(1): p. e37-e46.
3. Goldenberg, R.L., et al., *Epidemiology and causes of preterm birth.* Lancet, 2008. **371**(9606): p. 75-84.
4. Romero, R., S.K. Dey, and S.J. Fisher, *Preterm labor: one syndrome, many causes.* Science, 2014. **345**(6198): p. 760-5.
5. Gibbs, R.S., et al., *A review of premature birth and subclinical infection.* Am J Obstet Gynecol, 1992. **166**(5): p. 1515-28.
6. Gomez, R., et al., *Premature labor and intra-amniotic infection. Clinical aspects and role of the cytokines in diagnosis and pathophysiology.* Clin Perinatol, 1995. **22**(2): p. 281-342.
7. Gonçalves, L.F., T. Chaiworapongsa, and R. Romero, *Intrauterine infection and prematurity.* Ment Retard Dev Disabil Res Rev, 2002. **8**(1): p. 3-13.
8. Keelan, J.A., et al., *Cytokines, prostaglandins and parturition--a review.* Placenta, 2003. **24 Suppl A**: p. S33-46.
9. Bastek, J.A., L.M. Gómez, and M.A. Elovitz, *The role of inflammation and infection in preterm birth.* Clin Perinatol, 2011. **38**(3): p. 385-406.
10. Agrawal, V. and E. Hirsch, *Intrauterine infection and preterm labor.* Semin Fetal Neonatal Med, 2012. **17**(1): p. 12-9.
11. Combs, C.A., et al., *Amniotic fluid infection, inflammation, and colonization in preterm labor with intact membranes.* Am J Obstet Gynecol, 2014. **210**(2): p. 125 e1-125 e15.
12. Romero, R., et al., *Evidence that intra-amniotic infections are often the result of an ascending invasion - a molecular microbiological study.* J Perinat Med, 2019. **47**(9): p. 915-931.
13. Theis, K.R., et al., *Microbial burden and inflammasome activation in amniotic fluid of patients with preterm prelabor rupture of membranes.* J Perinat Med, 2020. **48**(2): p. 115-131.
14. Gibbs, R.S., et al., *Quantitative bacteriology of amniotic fluid from women with clinical intraamniotic infection at term.* J Infect Dis, 1982. **145**(1): p. 1-8.
15. Gravett, M.G., et al., *Preterm labor associated with subclinical amniotic fluid infection and with bacterial vaginosis.* Obstet Gynecol, 1986. **67**(2): p. 229-37.
16. Romero, R., et al., *Infection and labor. V. Prevalence, microbiology, and clinical significance of intraamniotic infection in women with preterm labor and intact membranes.* Am J Obstet Gynecol, 1989. **161**(3): p. 817-24.
17. Yoon, B.H., J.W. Chang, and R. Romero, *Isolation of Ureaplasma urealyticum from the amniotic cavity and adverse outcome in preterm labor.* Obstet Gynecol, 1998. **92**(1): p. 77-82.
18. DiGiulio, D.B., et al., *Prevalence and diversity of microbes in the amniotic fluid, the fetal inflammatory response, and pregnancy outcome in women with preterm pre-labor rupture of membranes.* Am J Reprod Immunol, 2010. **64**(1): p. 38-57.

19. Romero, R., et al., *A novel molecular microbiologic technique for the rapid diagnosis of microbial invasion of the amniotic cavity and intra-amniotic infection in preterm labor with intact membranes.* Am J Reprod Immunol, 2014. **71**(4): p. 330-58.
20. Romero, R., et al., *Clinical chorioamnionitis at term I: microbiology of the amniotic cavity using cultivation and molecular techniques.* J Perinat Med, 2015. **43**(1): p. 19-36.
21. Romero, R., et al., *Sterile intra-amniotic inflammation in asymptomatic patients with a sonographic short cervix: prevalence and clinical significance.* J Matern Fetal Neonatal Med, 2015. **28**(11): p. 1343-1359.
22. Romero, R., et al., *Sterile and microbial-associated intra-amniotic inflammation in preterm prelabor rupture of membranes.* J Matern Fetal Neonatal Med, 2015. **28**(12): p. 1394-409.
23. Oh, K.J., et al., *Evidence that antibiotic administration is effective in the treatment of a subset of patients with intra-amniotic infection/inflammation presenting with cervical insufficiency.* Am J Obstet Gynecol, 2019. **221**(2): p. 140.e1-140.e18.
24. Yoon, B.H., et al., *Antibiotic administration can eradicate intra-amniotic infection or intra-amniotic inflammation in a subset of patients with preterm labor and intact membranes.* Am J Obstet Gynecol, 2019. **221**(2): p. 142.e1-142.e22.
25. Burnham, P., et al., *Separating the signal from the noise in metagenomic cell-free DNA sequencing.* Microbiome, 2020. **8**(1): p. 18.
26. Romero, R., et al., *Amniotic fluid white blood cell count: a rapid and simple test to diagnose microbial invasion of the amniotic cavity and predict preterm delivery.* Am J Obstet Gynecol, 1991. **165**(4 Pt 1): p. 821-30.
27. Romero, R., et al., *The diagnostic and prognostic value of amniotic fluid white blood cell count, glucose, interleukin-6, and gram stain in patients with preterm labor and intact membranes.* Am J Obstet Gynecol, 1993. **169**(4): p. 805-16.
28. Romero, R., et al., *A comparative study of the diagnostic performance of amniotic fluid glucose, white blood cell count, interleukin-6, and gram stain in the detection of microbial invasion in patients with preterm premature rupture of membranes.* Am J Obstet Gynecol, 1993. **169**(4): p. 839-51.
29. Gomez, R., et al., *The value of amniotic fluid interleukin-6, white blood cell count, and gram stain in the diagnosis of microbial invasion of the amniotic cavity in patients at term.* Am J Reprod Immunol, 1994. **32**(3): p. 200-10.
30. Yoon, B.H., et al., *Maternal blood C-reactive protein, white blood cell count, and temperature in preterm labor: a comparison with amniotic fluid white blood cell count.* Obstet Gynecol, 1996. **87**(2): p. 231-7.
31. Gomez-Lopez, N., et al., *Are amniotic fluid neutrophils in women with intraamniotic infection and/or inflammation of fetal or maternal origin?* Am J Obstet Gynecol, 2017. **217**(6): p. 693.e1-693.e16.
32. Martinez-Varea, A., et al., *Clinical chorioamnionitis at term VII: the amniotic fluid cellular immune response.* J Perinat Med, 2017. **45**(5): p. 523-538.
33. Gomez-Lopez, N., et al., *The immunophenotype of amniotic fluid leukocytes in normal and complicated pregnancies.* Am J Reprod Immunol, 2018. **79**(4): p. e12827.
34. Gomez-Lopez, N., et al., *Fetal T Cell Activation in the Amniotic Cavity during Preterm Labor: A Potential Mechanism for a Subset of Idiopathic Preterm Birth.* J Immunol, 2019. **203**(7): p. 1793-1807.

35. Gomez-Lopez, N., et al., *The origin of amniotic fluid monocytes/macrophages in women with intra-amniotic inflammation or infection.* J Perinat Med, 2019. **47**(8): p. 822-840.
36. Gomez-Lopez, N., et al., *Cellular immune responses in amniotic fluid of women with preterm labor and intra-amniotic infection or intra-amniotic inflammation.* Am J Reprod Immunol, 2019. **82**(5): p. e13171.
37. Galaz, J., et al., *Cellular immune responses in amniotic fluid of women with preterm clinical chorioamnionitis.* Inflamm Res, 2020. **69**(2): p. 203-216.
38. Galaz, J., et al., *Cellular immune responses in amniotic fluid of women with preterm prelabor rupture of membranes.* J Perinat Med, 2020. **48**(3): p. 222-233.
39. Gomez-Lopez, N., et al., *RNA Sequencing Reveals Diverse Functions of Amniotic Fluid Neutrophils and Monocytes/Macrophages in Intra-Amniotic Infection.* J Innate Immun, 2021. **13**(2): p. 63-82.
40. Olding, L., *Value of placentitis as a sign of intrauterine infection in human subjects.* Acta Pathol Microbiol Scand A, 1970. **78**(3): p. 256-64.
41. Zhang, J.M., F.T. Kraus, and T.I. Aquino, *Chorioamnionitis: a comparative histologic, bacteriologic, and clinical study.* Int J Gynecol Pathol, 1985. **4**(1): p. 1-10.
42. Guzick, D.S. and K. Winn, *The association of chorioamnionitis with preterm delivery.* Obstet Gynecol, 1985. **65**(1): p. 11-6.
43. Svensson, L., I. Ingemarsson, and P.A. Mårdh, *Chorioamnionitis and the isolation of microorganisms from the placenta.* Obstet Gynecol, 1986. **67**(3): p. 403-9.
44. Hillier, S.L., et al., *A case-control study of chorioamnionic infection and histologic chorioamnionitis in prematurity.* N Engl J Med, 1988. **319**(15): p. 972-8.
45. van Hoeven, K.H., et al., *Clinical significance of increasing histologic severity of acute inflammation in the fetal membranes and umbilical cord.* Pediatr Pathol Lab Med, 1996. **16**(5): p. 731-44.
46. Odibo, A.O., et al., *Relationship of amniotic fluid markers of intra-amniotic infection with histopathology in cases of preterm labor with intact membranes.* J Perinatol, 1999. **19**(6 Pt 1): p. 407-12.
47. Yoon, B.H., et al., *Clinical significance of intra-amniotic inflammation in patients with preterm labor and intact membranes.* Am J Obstet Gynecol, 2001. **185**(5): p. 1130-6.
48. Pacora, P., et al., *Funisitis and chorionic vasculitis: the histological counterpart of the fetal inflammatory response syndrome.* J Matern Fetal Neonatal Med, 2002. **11**(1): p. 18-25.
49. Redline, R.W., et al., *Amniotic infection syndrome: nosology and reproducibility of placental reaction patterns.* Pediatr Dev Pathol, 2003. **6**(5): p. 435-48.
50. Kim, M.J., et al., *Widespread microbial invasion of the chorioamniotic membranes is a consequence and not a cause of intra-amniotic infection.* Lab Invest, 2009. **89**(8): p. 924-36.
51. Park, C.W., et al., *The involvement of human amnion in histologic chorioamnionitis is an indicator that a fetal and an intra-amniotic inflammatory response is more likely and severe: clinical implications.* Placenta, 2009. **30**(1): p. 56-61.
52. Oh, K.J., et al., *Predictive value of intra-amniotic and serum markers for inflammatory lesions of preterm placenta.* Placenta, 2011. **32**(10): p. 732-6.
53. Redline, R.W., *Inflammatory response in acute chorioamnionitis.* Semin Fetal Neonatal Med, 2012. **17**(1): p. 20-5.

54. Kim, C.J., et al., *Acute chorioamnionitis and funisitis: definition, pathologic features, and clinical significance.* Am J Obstet Gynecol, 2015. **213**(4 Suppl): p. S29-52.
55. Kim, S.M., et al., *The relationship between the intensity of intra-amniotic inflammation and the presence and severity of acute histologic chorioamnionitis in preterm gestation.* J Matern Fetal Neonatal Med, 2015. **28**(13): p. 1500-9.
56. Gomez-Lopez, N., et al., *Neutrophil extracellular traps in acute chorioamnionitis: A mechanism of host defense.* Am J Reprod Immunol, 2017. **77**(3).
57. Oh, J.W., et al., *Acute chorioamnionitis and intra-amniotic inflammation are more severe according to outside-in neutrophil migration within the same chorio-decidua.* Taiwan J Obstet Gynecol, 2021. **60**(4): p. 639-652.
58. Keski-Nisula, L.T., et al., *Myometrial inflammation in human delivery and its association with labor and infection.* Am J Clin Pathol, 2003. **120**(2): p. 217-24.
59. Makieva, S., et al., *The preterm cervix reveals a transcriptomic signature in the presence of premature prelabor rupture of membranes.* Am J Obstet Gynecol, 2017. **216**(6): p. 602 e1-602 e21.
60. Migale, R., et al., *Modeling hormonal and inflammatory contributions to preterm and term labor using uterine temporal transcriptomics.* BMC Med, 2016. **14**(1): p. 86.
61. Willcockson, A.R., et al., *Transcriptome signature identifies distinct cervical pathways induced in lipopolysaccharide-mediated preterm birth.* Biol Reprod, 2018. **98**(3): p. 408-421.
62. Motomura, K., et al., *Pregnancy-specific transcriptional changes upon endotoxin exposure in mice.* J Perinat Med, 2020. **48**(7): p. 700-722.
63. Toothaker, J.M., et al., *Immune Cells in the Placental Villi Contribute to Intra-amniotic Inflammation.* Front Immunol, 2020. **11**: p. 866.
64. Nelson, A.C., et al., *Single-cell RNA-seq reveals cell type-specific transcriptional signatures at the maternal-foetal interface during pregnancy.* Nat Commun, 2016. **7**: p. 11414.
65. Pavličev, M., et al., *Single-cell transcriptomics of the human placenta: inferring the cell communication network of the maternal-fetal interface.* Genome Res, 2017. **27**(3): p. 349-361.
66. Tsang, J.C.H., et al., *Integrative single-cell and cell-free plasma RNA transcriptomics elucidates placental cellular dynamics.* Proc Natl Acad Sci U S A, 2017. **114**(37): p. E7786-e7795.
67. Vento-Tormo, R., et al., *Single-cell reconstruction of the early maternal-fetal interface in humans.* Nature, 2018. **563**(7731): p. 347-353.
68. Suryawanshi, H., et al., *A single-cell survey of the human first-trimester placenta and decidua.* Sci Adv, 2018. **4**(10): p. eaau4788.
69. Pique-Regi, R., et al., *Single cell transcriptional signatures of the human placenta in term and preterm parturition.* Elife, 2019. **8**.
70. Huang, J., et al., *Single-cell RNA sequencing reveals heterogeneity and differential expression of decidual tissues during the peripartum period.* Cell Prolif, 2021. **54**(2): p. e12967.
71. Pique-Regi, R., et al., *A single-cell atlas of the myometrium in human parturition.* JCI Insight, 2022. **7**(5).

72. Tarca, A.L., et al., *Targeted expression profiling by RNA-Seq improves detection of cellular dynamics during pregnancy and identifies a role for T cells in term parturition.* Sci Rep, 2019. **9**(1): p. 848.
73. Tarca, A.L., et al., *Maternal whole blood mRNA signatures identify women at risk of early preeclampsia: a longitudinal study.* J Matern Fetal Neonatal Med, 2021. **34**(21): p. 3463-3474.
74. Gomez-Lopez, N., et al., *Transcriptome changes in maternal peripheral blood during term parturition mimic perturbations preceding spontaneous preterm birth.* Biol Reprod, 2022. **106**(1): p. 185-199.
75. Senthamaraikannan, P., et al., *Intra-amniotic Ureaplasma parvum-Induced Maternal and Fetal Inflammation and Immune Responses in Rhesus Macaques.* J Infect Dis, 2016. **214**(10): p. 1597-1604.
76. Faro, J., et al., *Intra-amniotic inflammation induces preterm birth by activating the NLRP3 inflammasome.* Biol Reprod, 2019. **100**(5): p. 1290-1305.
77. Motomura, K., et al., *Intra-Amniotic Infection with Ureaplasma parvum Causes Preterm Birth and Neonatal Mortality That Are Prevented by Treatment with Clarithromycin.* mBio, 2020. **11**(3).
78. Motomura, K., et al., *RNA Sequencing Reveals Distinct Immune Responses in the Chorioamniotic Membranes of Women with Preterm Labor and Microbial or Sterile Intra-amniotic Inflammation.* Infect Immun, 2021. **89**(5).
79. Yoneda, N., et al., *Polymicrobial Amniotic Fluid Infection with Mycoplasma/Ureaplasma and Other Bacteria Induces Severe Intra-Amniotic Inflammation Associated with Poor Perinatal Prognosis in Preterm Labor.* Am J Reprod Immunol, 2016. **75**(2): p. 112-25.
80. Romero, R., et al., *The preterm labor syndrome.* Ann N Y Acad Sci, 1994. **734**: p. 414-29.
81. Norwitz, E.R., J.N. Robinson, and J.R. Challis, *The control of labor.* N Engl J Med, 1999. **341**(9): p. 660-6.
82. Lopez Bernal, A., *Mechanisms of labour--biochemical aspects.* BJOG, 2003. **110 Suppl 20**: p. 39-45.
83. Romero, R., et al., *The preterm parturition syndrome.* BJOG, 2006. **113 Suppl 3**: p. 17-42.
84. Smith, R., *Parturition.* N Engl J Med, 2007. **356**(3): p. 271-83.
85. Trundley, A. and A. Moffett, *Human uterine leukocytes and pregnancy.* Tissue Antigens, 2004. **63**(1): p. 1-12.
86. Erlebacher, A., *Immunology of the maternal-fetal interface.* Annu Rev Immunol, 2013. **31**: p. 387-411.
87. Bartmann, C., et al., *Quantification of the predominant immune cell populations in decidua throughout human pregnancy.* Am J Reprod Immunol, 2014. **71**(2): p. 109-19.
88. Li, Y., et al., *Decidual-Placental Immune Landscape During Syngeneic Murine Pregnancy.* Front Immunol, 2018. **9**: p. 2087.
89. Koh, W., et al., *Single Cell Transcriptomes Derived from Human Cervical and Uterine Tissue during Pregnancy.* Adv Biosyst, 2019. **3**(11): p. e1800336.
90. Chumduri, C., et al., *Opposing Wnt signals regulate cervical squamocolumnar homeostasis and emergence of metaplasia.* Nat Cell Biol, 2021. **23**(2): p. 184-197.
91. Zhao, Z., et al., *Single-cell analysis defines the lineage plasticity of stem cells in cervix epithelium.* Cell Regen, 2021. **10**(1): p. 36.

92. Osman, I., et al., *Leukocyte density and pro-inflammatory cytokine expression in human fetal membranes, decidua, cervix and myometrium before and during labour at term.* Mol Hum Reprod, 2003. **9**(1): p. 41-5.
93. Timmons, B.C., A.M. Fairhurst, and M.S. Mahendroo, *Temporal changes in myeloid cells in the cervix during pregnancy and parturition.* J Immunol, 2009. **182**(5): p. 2700-7.
94. Dobyns, A.E., et al., *Macrophage gene expression associated with remodeling of the prepartum rat cervix: microarray and pathway analyses.* PLoS One, 2015. **10**(3): p. e0119782.
95. Dubicke, A., et al., *Density of Stromal Cells and Macrophages Associated With Collagen Remodeling in the Human Cervix in Preterm and Term Birth.* Reprod Sci, 2016. **23**(5): p. 595-603.
96. Vargas, M.L., et al., *Comparison of the proportions of leukocytes in early and term human decidua.* Am J Reprod Immunol, 1993. **29**(3): p. 135-40.
97. Sindram-Trujillo, A., et al., *Increased T-cell activation in decidua parietalis compared to decidua basalis in uncomplicated human term pregnancy.* Am J Reprod Immunol, 2003. **49**(5): p. 261-8.
98. Gomez-Lopez, N., et al., *Fetal membranes exhibit selective leukocyte chemotaxic activity during human labor.* J Reprod Immunol, 2009. **80**(1-2): p. 122-31.
99. Gomez-Lopez, N., et al., *Specific inflammatory microenvironments in the zones of the fetal membranes at term delivery.* Am J Obstet Gynecol, 2011. **205**(3): p. 235.e15-24.
100. Gomez-Lopez, N., et al., *Choriodecidua and amnion exhibit selective leukocyte chemotaxis during term human labor.* Am J Obstet Gynecol, 2011. **204**(4): p. 364.e9-16.
101. Gomez-Lopez, N., et al., *Evidence for a role for the adaptive immune response in human term parturition.* Am J Reprod Immunol, 2013. **69**(3): p. 212-30.
102. Arenas-Hernandez, M., et al., *Effector and Activated T Cells Induce Preterm Labor and Birth That Is Prevented by Treatment with Progesterone.* J Immunol, 2019. **202**(9): p. 2585-2608.
103. Slutsky, R., et al., *Exhausted and Senescent T Cells at the Maternal-Fetal Interface in Preterm and Term Labor.* J Immunol Res, 2019. **2019**: p. 3128010.
104. Huang, J.R., et al., *Single-cell transcriptomics reveals the heterogeneity of the decidual endothelial cells that participate in labor onset.* Eur Rev Med Pharmacol Sci, 2020. **24**(20): p. 10359-10365.
105. Akgul, Y., et al., *Hyaluronan in cervical epithelia protects against infection-mediated preterm birth.* J Clin Invest, 2014. **124**(12): p. 5481-9.
106. Pavlidis, I., et al., *Cervical epithelial damage promotes Ureaplasma parvum ascending infection, intrauterine inflammation and preterm birth induction in mice.* Nat Commun, 2020. **11**(1): p. 199.
107. Danforth, D.N. and A.C. Ivy, *The lower uterine segment; its derivation and physiologic behavior.* Am J Obstet Gynecol, 1949. **57**(5): p. 831-41.
108. Schwalm, H. and V. Dubrauszky, *The structure of the musculature of the human uterus--muscles and connective tissue.* Am J Obstet Gynecol, 1966. **94**(3): p. 391-404.
109. Wikland, M., et al., *Oxytocin, prostaglandins, and contractility of the human uterus at term pregnancy.* Acta Obstet Gynecol Scand, 1982. **61**(5): p. 467-72.
110. Sparey, C., et al., *The differential expression of myometrial connexin-43, cyclooxygenase-1 and -2, and Gs alpha proteins in the upper and lower segments of the human uterus during pregnancy and labor.* J Clin Endocrinol Metab, 1999. **84**(5): p. 1705-10.

111. Pollard, A.J., et al., *Spatio-temporal expression of the trans-acting splicing factors SF2/ASF and heterogeneous ribonuclear proteins A1/A1B in the myometrium of the pregnant human uterus: a molecular mechanism for regulating regional protein isoform expression in vivo.* J Clin Endocrinol Metab, 2000. **85**(5): p. 1928-36.
112. Bukowski, R., et al., *Labor-associated gene expression in the human uterine fundus, lower segment, and cervix.* PLoS Med, 2006. **3**(6): p. e169.
113. Sooranna, S.R., et al., *Myometrial prostaglandin E2 synthetic enzyme mRNA expression: spatial and temporal variations with pregnancy and labour.* Mol Hum Reprod, 2006. **12**(10): p. 625-31.
114. Mosher, A.A., et al., *Development and validation of primary human myometrial cell culture models to study pregnancy and labour.* BMC Pregnancy Childbirth, 2013. **13 Suppl 1**(Suppl 1): p. S7.
115. Liu, L., et al., *HoxA13 Regulates Phenotype Regionalization of Human Pregnant Myometrium.* J Clin Endocrinol Metab, 2015. **100**(12): p. E1512-22.
116. Patwardhan, M., et al., *Dynamic Changes in the Myometrium during the Third Stage of Labor, Evaluated Using Two-Dimensional Ultrasound, in Women with Normal and Abnormal Third Stage of Labor and in Women with Obstetric Complications.* Gynecol Obstet Invest, 2015. **80**(1): p. 26-37.
117. Jin, S., et al., *Inference and analysis of cell-cell communication using CellChat.* Nat Commun, 2021. **12**(1): p. 1088.
118. Bollapragada, S., et al., *Term labor is associated with a core inflammatory response in human fetal membranes, myometrium, and cervix.* Am J Obstet Gynecol, 2009. **200**(1): p. 104.e1-11.
119. Mittal, P., et al., *Characterization of the myometrial transcriptome and biological pathways of spontaneous human labor at term.* J Perinat Med, 2010. **38**(6): p. 617-43.
120. Chan, Y.W., et al., *Assessment of myometrial transcriptome changes associated with spontaneous human labour by high-throughput RNA-seq.* Exp Physiol, 2014. **99**(3): p. 510-24.
121. Stanfield, Z., et al., *Myometrial Transcriptional Signatures of Human Parturition.* Front Genet, 2019. **10**: p. 185.
122. Gershater, M., et al., *IL-22 Plays a Dual Role in the Amniotic Cavity: Tissue Injury and Host Defense against Microbes in Preterm Labor.* J Immunol, 2022.
123. Ito, M., et al., *A role for IL-17 in induction of an inflammation at the fetomaternal interface in preterm labour.* J Reprod Immunol, 2010. **84**(1): p. 75-85.
124. Sakamoto, Y., et al., *Macrophages and not granulocytes are involved in cervical ripening.* J Reprod Immunol, 2005. **66**(2): p. 161-73.
125. Gonzalez, J.M., et al., *Cervical remodeling/ripening at term and preterm delivery: the same mechanism initiated by different mediators and different effector cells.* PLoS One, 2011. **6**(11): p. e26877.
126. Payne, K.J., et al., *Residency and activation of myeloid cells during remodeling of the prepartum murine cervix.* Biol Reprod, 2012. **87**(5): p. 106.
127. Krantz, K.E. and W.P. Phillips, *Anatomy of the human uterine cervix, gross and microscopic.* Ann N Y Acad Sci, 1962. **97**: p. 551-63.
128. Granstrom, L., et al., *Changes in the connective tissue of corpus and cervix uteri during ripening and labour in term pregnancy.* Br J Obstet Gynaecol, 1989. **96**(10): p. 1198-202.

129. Ludmir, J. and H.M. Sehdev, *Anatomy and physiology of the uterine cervix.* Clin Obstet Gynecol, 2000. **43**(3): p. 433-9.
130. Montes, G.S., et al., *Phenotypic modulation of fibroblastic cells in the mucous layer of the human uterine cervix at term.* Reproduction, 2002. **124**(6): p. 783-90.
131. Varayoud, J., et al., *Characterization of fibroblastic cell plasticity in the lamina propria of the rat uterine cervix at term.* Biol Reprod, 2001. **65**(2): p. 375-83.
132. Vink, J.Y., et al., *A new paradigm for the role of smooth muscle cells in the human cervix.* Am J Obstet Gynecol, 2016. **215**(4): p. 478 e1-478 e11.
133. Romero, R., et al., *Infection and labor. III. Interleukin-1: a signal for the onset of parturition.* Am J Obstet Gynecol, 1989. **160**(5 Pt 1): p. 1117-23.
134. Romero, R., et al., *Interleukin-1 stimulates prostaglandin biosynthesis by human amnion.* Prostaglandins, 1989. **37**(1): p. 13-22.
135. Bry, K. and M. Hallman, *Synergistic stimulation of amnion cell prostaglandin E2 synthesis by interleukin-1, tumor necrosis factor and products from activated human granulocytes.* Prostaglandins Leukot Essent Fatty Acids, 1991. **44**(4): p. 241-5.
136. Romero, R., et al., *Interleukin-1 alpha and interleukin-1 beta in preterm and term human parturition.* Am J Reprod Immunol, 1992. **27**(3-4): p. 117-23.
137. Goldenberg, R.L., J.C. Hauth, and W.W. Andrews, *Intrauterine infection and preterm delivery.* N Engl J Med, 2000. **342**(20): p. 1500-7.
138. Romero, R., et al., *The role of infection in preterm labour and delivery.* Paediatr Perinat Epidemiol, 2001. **15 Suppl 2**: p. 41-56.
139. Romero, R., et al., *Inflammation in preterm and term labour and delivery.* Semin Fetal Neonatal Med, 2006. **11**(5): p. 317-26.
140. Gomez-Lopez, N., et al., *Intra-amniotic administration of lipopolysaccharide induces spontaneous preterm labor and birth in the absence of a body temperature change.* J Matern Fetal Neonatal Med, 2018. **31**(4): p. 439-446.
141. Garcia-Flores, V., et al., *Inflammation-Induced Adverse Pregnancy and Neonatal Outcomes Can Be Improved by the Immunomodulatory Peptide Exendin-4.* Front Immunol, 2018. **9**: p. 1291.
142. Ledger, W.J., *Infection and premature labor.* Am J Perinatol, 1989. **6**(2): p. 234-6.
143. Graham, J.M., et al., *Uterine contractions after antibiotic therapy for pyelonephritis in pregnancy.* Am J Obstet Gynecol, 1993. **168**(2): p. 577-80.
144. Kaul, A.K., et al., *Experimental gestational pyelonephritis induces preterm births and low birth weights in C3H/HeJ mice.* Infect Immun, 1999. **67**(11): p. 5958-66.
145. Millar, L.K., L. DeBuque, and D.A. Wing, *Uterine contraction frequency during treatment of pyelonephritis in pregnancy and subsequent risk of preterm birth.* J Perinat Med, 2003. **31**(1): p. 41-6.
146. Jolley, J.A., S. Kim, and D.A. Wing, *Acute pyelonephritis and associated complications during pregnancy in 2006 in US hospitals.* J Matern Fetal Neonatal Med, 2012. **25**(12): p. 2494-8.
147. Dawkins, J.C., et al., *Acute pyelonephritis in pregnancy: a retrospective descriptive hospital based-study.* ISRN Obstet Gynecol, 2012. **2012**: p. 519321.
148. Wendremaire, M., et al., *Macrophage-induced reactive oxygen species promote myometrial contraction and labor-associated mechanisms.* Biol Reprod, 2020. **102**(6): p. 1326-1339.

149. Coleman, M., et al., *A Broad Spectrum Chemokine Inhibitor Prevents Preterm Labor but Not Microbial Invasion of the Amniotic Cavity or Neonatal Morbidity in a Non-human Primate Model.* Front Immunol, 2020. **11**: p. 770.
150. Boros-Rausch, A., O. Shynlova, and S.J. Lye, *A Broad-Spectrum Chemokine Inhibitor Blocks Inflammation-Induced Myometrial Myocyte-Macrophage Crosstalk and Myometrial Contraction.* Cells, 2021. **11**(1).
151. Dobin, A., et al., *STAR: ultrafast universal RNA-seq aligner.* Bioinformatics, 2013. **29**(1): p. 15-21.
152. Kang, H.M., et al., *Multiplexed droplet single-cell RNA-sequencing using natural genetic variation.* Nat Biotechnol, 2018. **36**(1): p. 89-94.
153. Young, M.D. and S. Behjati, *SoupX removes ambient RNA contamination from droplet-based single-cell RNA sequencing data.* Gigascience, 2020. **9**(12).
154. McGinnis, C.S., L.M. Murrow, and Z.J. Gartner, *DoubletFinder: Doublet Detection in Single-Cell RNA Sequencing Data Using Artificial Nearest Neighbors.* Cell Syst, 2019. **8**(4): p. 329-337 e4.
155. Stuart, T., et al., *Comprehensive Integration of Single-Cell Data.* Cell, 2019. **177**(7): p. 1888-1902 e21.
156. Hafemeister, C. and R. Satija, *Normalization and variance stabilization of single-cell RNA-seq data using regularized negative binomial regression.* Genome Biol, 2019. **20**(1): p. 296.
157. Korsunsky, I., et al., *Fast, sensitive and accurate integration of single-cell data with Harmony.* Nat Methods, 2019. **16**(12): p. 1289-1296.
158. McInnes, L., J. Healy, and J. Melville *UMAP: Uniform Manifold Approximation and Projection for Dimension Reduction.* 2018. arXiv:1802.03426.
159. Becht, E., et al., *Dimensionality reduction for visualizing single-cell data using UMAP.* Nat Biotechnol, 2018.
160. Aran, D., et al., *Reference-based analysis of lung single-cell sequencing reveals a transitional profibrotic macrophage.* Nat Immunol, 2019. **20**(2): p. 163-172.
161. Tabula Muris, C., et al., *Single-cell transcriptomics of 20 mouse organs creates a Tabula Muris.* Nature, 2018. **562**(7727): p. 367-372.
162. Buechler, M.B., et al., *Cross-tissue organization of the fibroblast lineage.* Nature, 2021. **593**(7860): p. 575-579.
163. Han, X., et al., *Mapping the Mouse Cell Atlas by Microwell-Seq.* Cell, 2018. **172**(5): p. 1091-1107 e17.
164. Love, M.I., W. Huber, and S. Anders, *Moderated estimation of fold change and dispersion for RNA-seq data with DESeq2.* Genome Biol, 2014. **15**(12): p. 550.
165. Yu, G., et al., *clusterProfiler: an R package for comparing biological themes among gene clusters.* OMICS, 2012. **16**(5): p. 284-7.

FIGURE LEGENDS

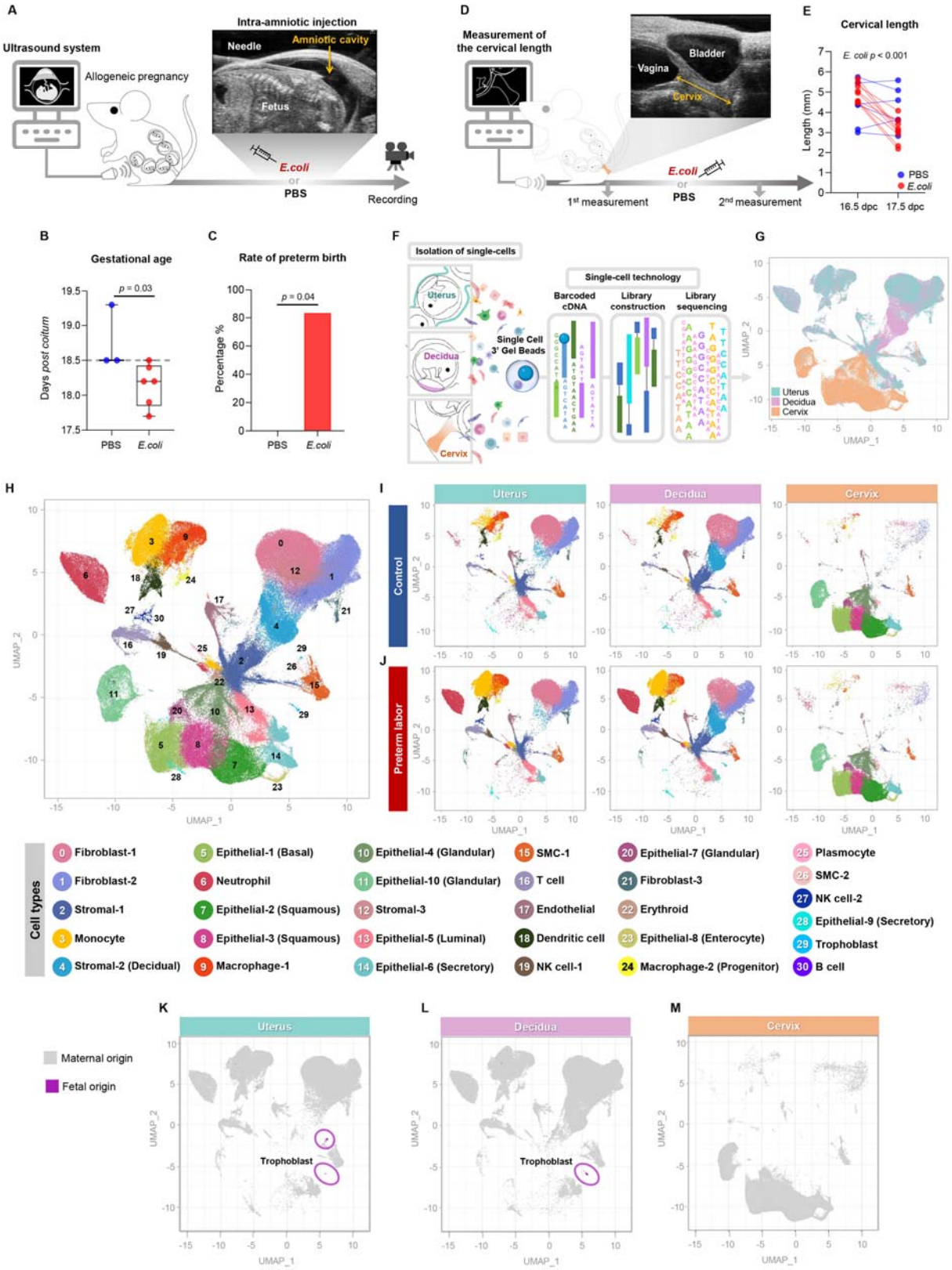

Figure 1. Preterm labor induced by intra-amniotic *Escherichia coli* alters the cellular composition of the reproductive tissues. (A) Experimental design for the ultrasound-guided intra-amniotic injection of *E. coli* or PBS (vehicle control) into pregnant mice on 16.5 days *post coitum* (dpc) (n = 3-6 per group). Mice were monitored to determine pregnancy outcomes **(B-C)**. Gestational age and preterm birth rate of dams intra-amniotically injected with *E. coli or* PBS. Grey dashed line corresponds to the cut-off for term delivery (≥18.5 dpc). Gestational age was compared using a 2-sided Mann-Whitney U-test, and preterm birth rates were compared using a 2-sided Fisher's test. $P < 0.05$ was considered significant. **(D)** Experimental design for the determination of cervical length on 16.5 dpc, prior to intra-amniotic injection of *E. coli* or PBS, and 24 h later (17.5 dpc) (n = 6-9 per group). **(E)** Cervical length of dams intra-amniotically injected with *E. coli* or PBS at 16.5 and 17.5 dpc. Cervical length was compared between time points using a 2-sided Mann-Whitney U-tests. $P < 0.05$ was considered significant. **(F)** Diagram illustrating the preparation of single-cell suspensions from the uterus, decidua, and cervix collected 24 h after *E. coli*-induced preterm labor (17.5 dpc) for single-cell RNA-sequencing (scRNA-seq) (n = 3 per group). **(G)** Color-coded uniform manifold approximation and projection (UMAP) plot showing tissue-specific predominance of distinct cell types in the uterus (blue), decidua (pink), and cervix (orange). **(H)** UMAP plot showing all cell types present in the uterus, decidua, and cervix. UMAP plots showing the cell types present in the uterus, decidua, and cervix of **(I)** control mice and **(J)** mice with preterm labor. **(K-M)** UMAP plots showing the distribution of cells according to fetal (purple) or maternal (grey) origin in the uterus, decidua, and cervix. Abbreviations used: SMC, smooth muscle cell; NK cell, natural killer cell.

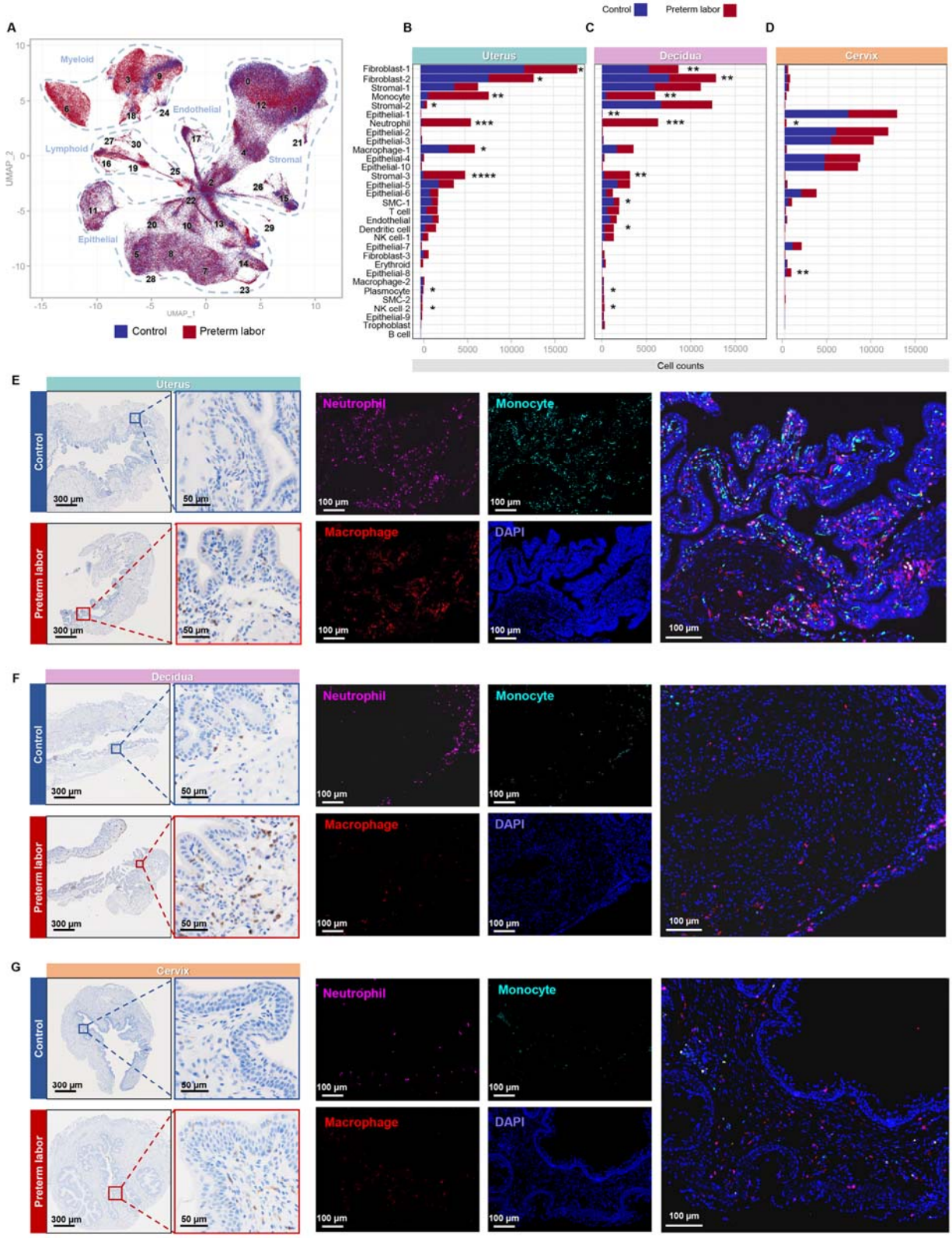
A
Myeloid
Endothelial
Lymphoid
Stromal
Epithelial
UMAP_1
UMAP_2
Control
Preterm labor
B
C
D
Control
Preterm labor
Uterus
Decidua
Cervix
Fibroblast-1
Fibroblast-2
Stromal-1
Monocyte
Stromal-2
Epithelial-1
Neutrophil
Epithelial-2
Epithelial-3
Macrophage-1
Epithelial-4
Epithelial-10
Stromal-3
Epithelial-5
Epithelial-6
SMC-1
T cell
Endothelial
Dendritic cell
NK cell-1
Epithelial-7
Fibroblast-3
Erythroid
Epithelial-8
Macrophage-2
Plasmocyte
SMC-2
NK cell-2
Epithelial-9
Trophoblast
B cell
Cell counts
E
Uterus
Control
Preterm labor
Neutrophil
Monocyte
Macrophage
DAPI
F
Decidua
G
Cervix
300 µm
50 µm
100 µm

1306

1307 **Figure 2**. **Preterm labor involves leukocyte infiltration in the reproductive tissues**. **(A)**
1308 Color-coded uniform manifold approximation and projection (UMAP) plot showing the effects
1309 of preterm labor on the abundance of specific cell types (shown in red) compared to control
1310 (shown in blue). Blue dotted lines distinguish major cell types: myeloid, endothelial, stromal,
1311 epithelial, and lymphoid. **(B-D)** Bar plots showing the numbers of each cell type in the uterus,
1312 decidua, and cervix. The comparison of cell numbers between the two study groups for each cell
1313 type was performed using a 2-sided t-test. * $p < 0.05$, ** $p < 0.01$, *** $p < 0.001$, **** $p <$
1314 0.0001. **(E-G)** Representative images showing 3, 3'diaminobenzidine (DAB)
1315 immunohistochemistry to detect the pan-leukocyte marker CD45 in the uterus, decidua, and
1316 cervix of control mice (top row) and mice with preterm labor (bottom row) (n = 3 per group).
1317 Whole-slide brightfield images taken at **(E)** control: 3.5X, preterm labor: 3.3X; **(F)** control:
1318 2.9X, preterm labor 3.9X; **(G)** control: 3.4X, preterm labor: 3.2X (scale bars = 300μm). Zoomed
1319 images were taken at 20X magnification (scale bars = 50μm). Representative images showing
1320 immunofluorescence detection of neutrophils (Ly6G+ cells, pink), monocytes (Ly6C+ cells,
1321 cyan), and macrophages (F4/80+ cells, red) in the uterus, decidua, and cervix of mice with
1322 preterm labor only (n = 3). Nuclear staining is shown in blue (4',6-diamidino-2-phenylindole;
1323 DAPI). Merged images show the co-localization of immune cell populations in each tissue.
1324 Images were scanned at 20X. Scale bar = 100μm. Abbreviations used: SMC, smooth muscle cell;
1325 NK cell, natural killer cell.
1326
1327

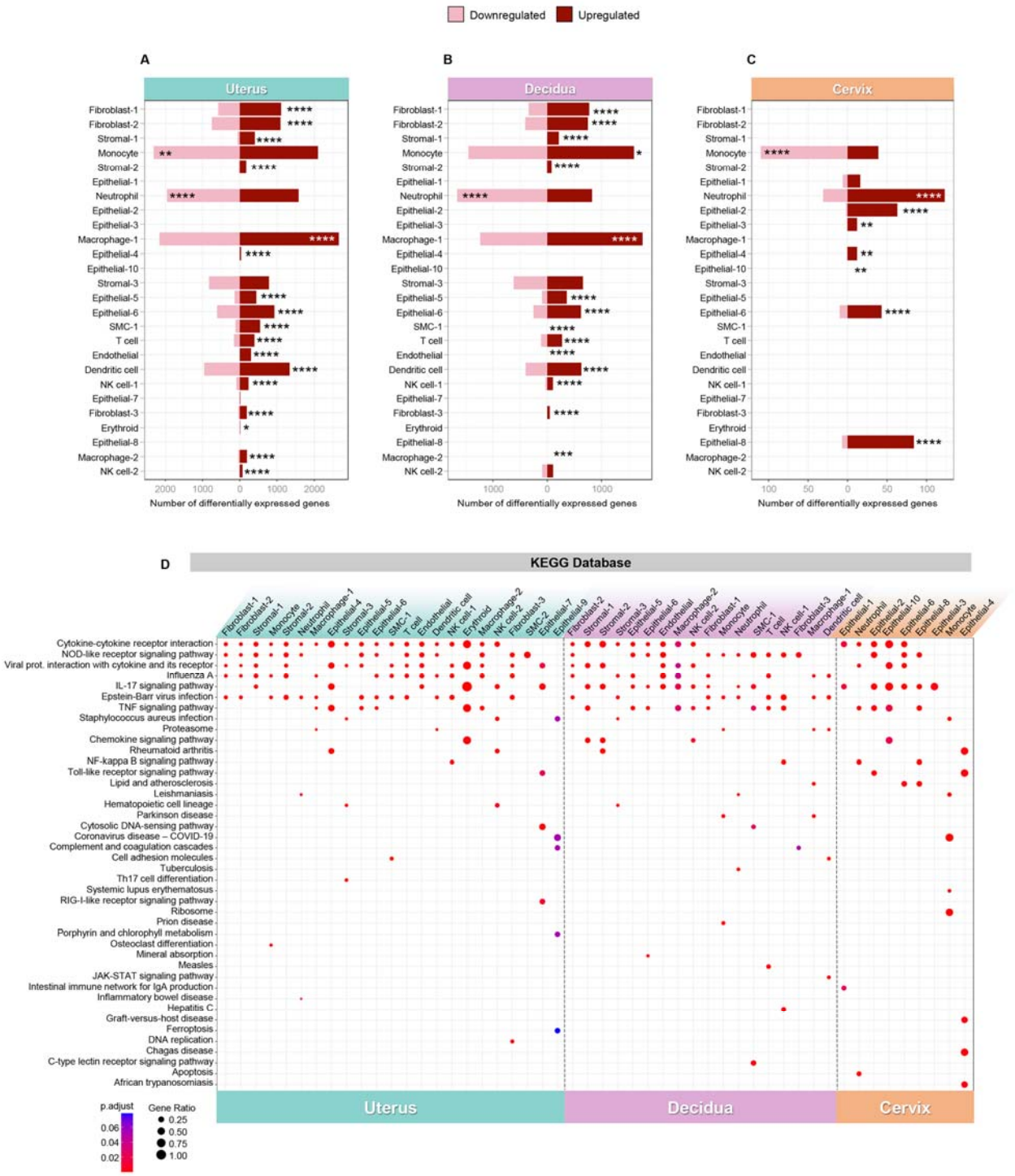

Figure 3. Preterm labor drives cell type-specific enrichment of immune-related processes in the reproductive tissues. (A-C) Bar plots showing the numbers of differentially expressed genes (DEGs) induced by preterm labor in each cell type in the uterus, decidua, and cervix. Red and pink bars indicate upregulated and downregulated DEGs, respectively (derived from

1333 DESeq2, $q < 0.1$). The comparisons of the fraction of downregulated and upregulated DEGs in
1334 each cell type between the study groups were calculated using two-sided binomial tests. * $q <$
1335 0.05, ** $q < 0.01$, *** $q < 0.001$, **** $q < 0.0001$. **(D)** ClusterProfiler dot plot showing preterm
1336 labor-associated Kyoto Encyclopedia of Genes and Genomes (KEGG) pathways enriched in
1337 specific cell types in the uterus, decidua, and cervix. The size and color of each dot represents
1338 enrichment score and significance level, respectively. Significant KEGG pathways ($q < 0.05$)
1339 were identified based on over-representation analysis using one-sided Fisher's exact tests.
1340 Abbreviations used: SMC, smooth muscle cell; NK cell, natural killer cell.
1341
1342

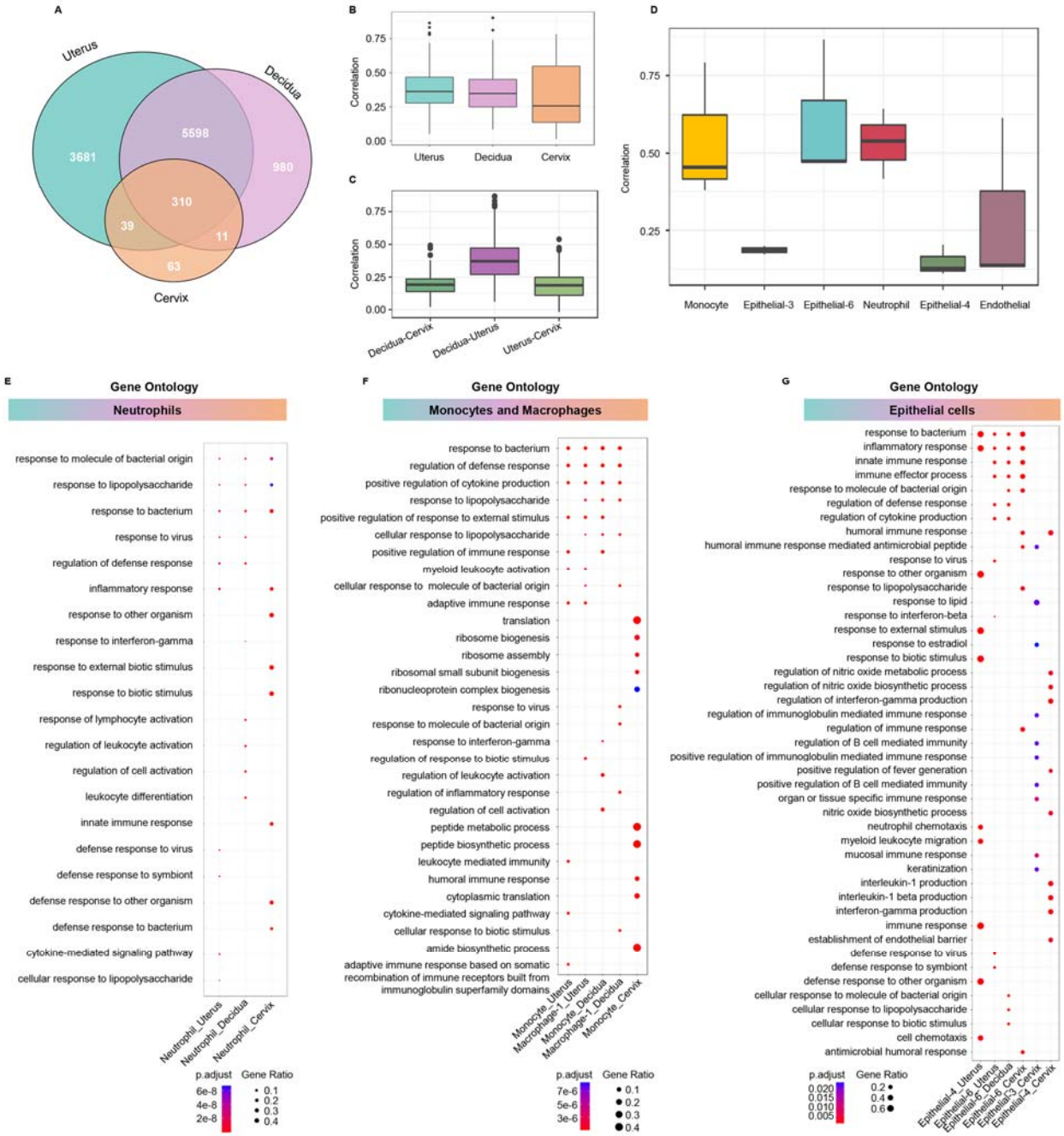

Figure 4. **Cell type-specific contributions to preterm labor in the reproductive tissues. (A)** Venn diagrams showing the numbers of differential expressed genes (DEGs, $q < 0.1$) that are unique to or shared among the uterus, decidua, and cervix. **(B)** Box plots showing the Spearman's correlation of the preterm labor-associated log(Fold change, FC) among cell types within each tissue. **(C)** Box plots showing the Spearman's correlations between tissue pairs for

1349 the preterm labor-associated logFC in cell types present in the two tissues. **(D)** Box plots
1350 showing the correlation of specific cell types affected by preterm labor and conserved across the
1351 uterus, decidua, and cervix using the Spearman's method. **(E-G)** Cluster profiler dot plots
1352 showing the preterm labor-associated Gene Ontology (GO) biological processes that are unique
1353 or shared among Neutrophil, Monocyte and Macrophage, and Epithelial cell types from the
1354 uterus, decidua, and cervix. The size and color of each dot represent gene ratio and significance
1355 level, respectively. 1-sided Fisher's exact tests were used.
1356
1357

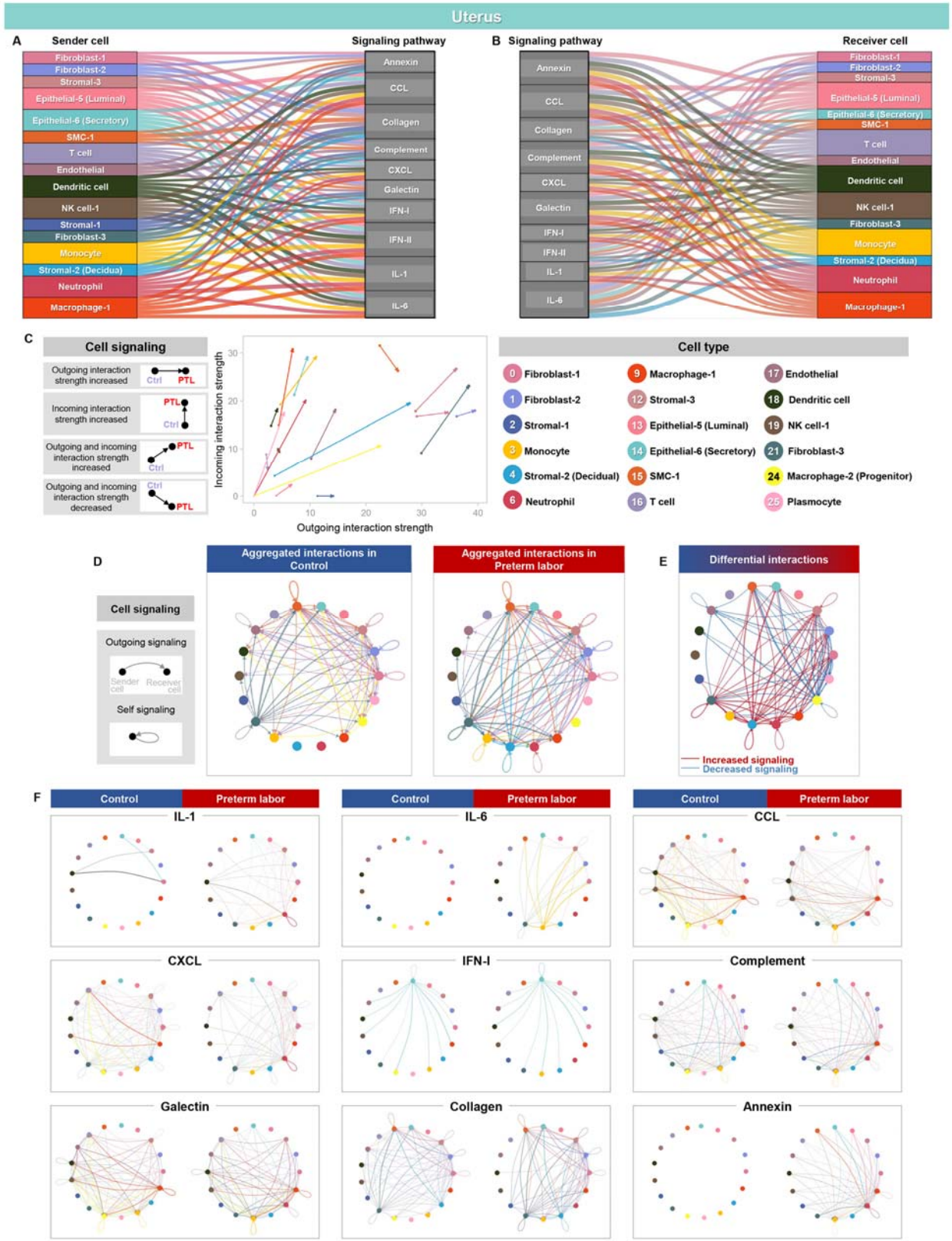
Uterus
A
Sender cell
Signaling pathway
Fibroblast-1
Fibroblast-2
Stromal-3
Epithelial-5 (Luminal)
Epithelial-6 (Secretory)
SMC-1
T cell
Endothelial
Dendritic cell
NK cell-1
Stromal-1
Fibroblast-3
Monocyte
Stromal-2 (Decidua)
Neutrophil
Macrophage-1
Annexin
CCL
Collagen
Complement
CXCL
Galectin
IFN-I
IFN-II
IL-1
IL-6
B
Signaling pathway
Receiver cell
C
Cell signaling
Outgoing interaction strength increased
Incoming interaction strength increased
Outgoing and incoming interaction strength increased
Outgoing and incoming interaction strength decreased
Ctrl
PTL
Incoming interaction strength
Outgoing interaction strength
Cell type
0 Fibroblast-1
1 Fibroblast-2
2 Stromal-1
3 Monocyte
4 Stromal-2 (Decidual)
6 Neutrophil
9 Macrophage-1
12 Stromal-3
13 Epithelial-5 (Luminal)
14 Epithelial-6 (Secretory)
15 SMC-1
16 T cell
17 Endothelial
18 Dendritic cell
19 NK cell-1
21 Fibroblast-3
24 Macrophage-2 (Progenitor)
25 Plasmocyte
D
Cell signaling
Outgoing signaling
Sender cell
Receiver cell
Self signaling
Aggregated interactions in Control
Aggregated interactions in Preterm labor
E
Differential interactions
Increased signaling
Decreased signaling
F
Control
Preterm labor
IL-1
IL-6
CCL
CXCL
IFN-I
Complement
Galectin
Collagen
Annexin

1358

1359 **Figure 5. Cellular interactions in the uterus during preterm labor. (A-B)** Alluvial plots
1360 showing the roles of specific cell types as senders or receivers of preterm labor-associated
1361 signaling in the uterus based on selected enriched signaling pathways comparing the overall
1362 information flow within networks between preterm labor and control derived from CellChat (full
1363 list of pathways in figure supplement 3B). Connecting lines are color-coded and represent the
1364 participation of each cell type as senders or receivers of the indicated signaling pathway. Line
1365 thickness is proportional to the strength of interaction. **(C)** Arrow plot showing changes in
1366 outgoing and incoming interactions strength between preterm labor (point of the arrow) and
1367 control condition (base of the arrow) for specific cell types in the uterus. **(D)** Circle plots
1368 showing the top 25% of aggregated interactions among cell types in the uterus for control and
1369 preterm labor groups. Each node represents a cell type and the interaction is shown by lines
1370 color-coded based on the sender cell. **(E)** Circle plot showing the top 25% increased (red) or
1371 decreased (blue) signaling interactions in the uterus in preterm labor compared to controls. **(F)**
1372 Circle plots representing the top 25% uterine cell-cell communications inferred for the IL-1, IL-
1373 6, CCL, CXCL, IFN-I, Complement, Galectin, Collagen, and Annexin pathways for the control
1374 and preterm labor groups. Abbreviations used: SMC, smooth muscle cell; NK cell, natural killer
1375 cell.
1376
1377

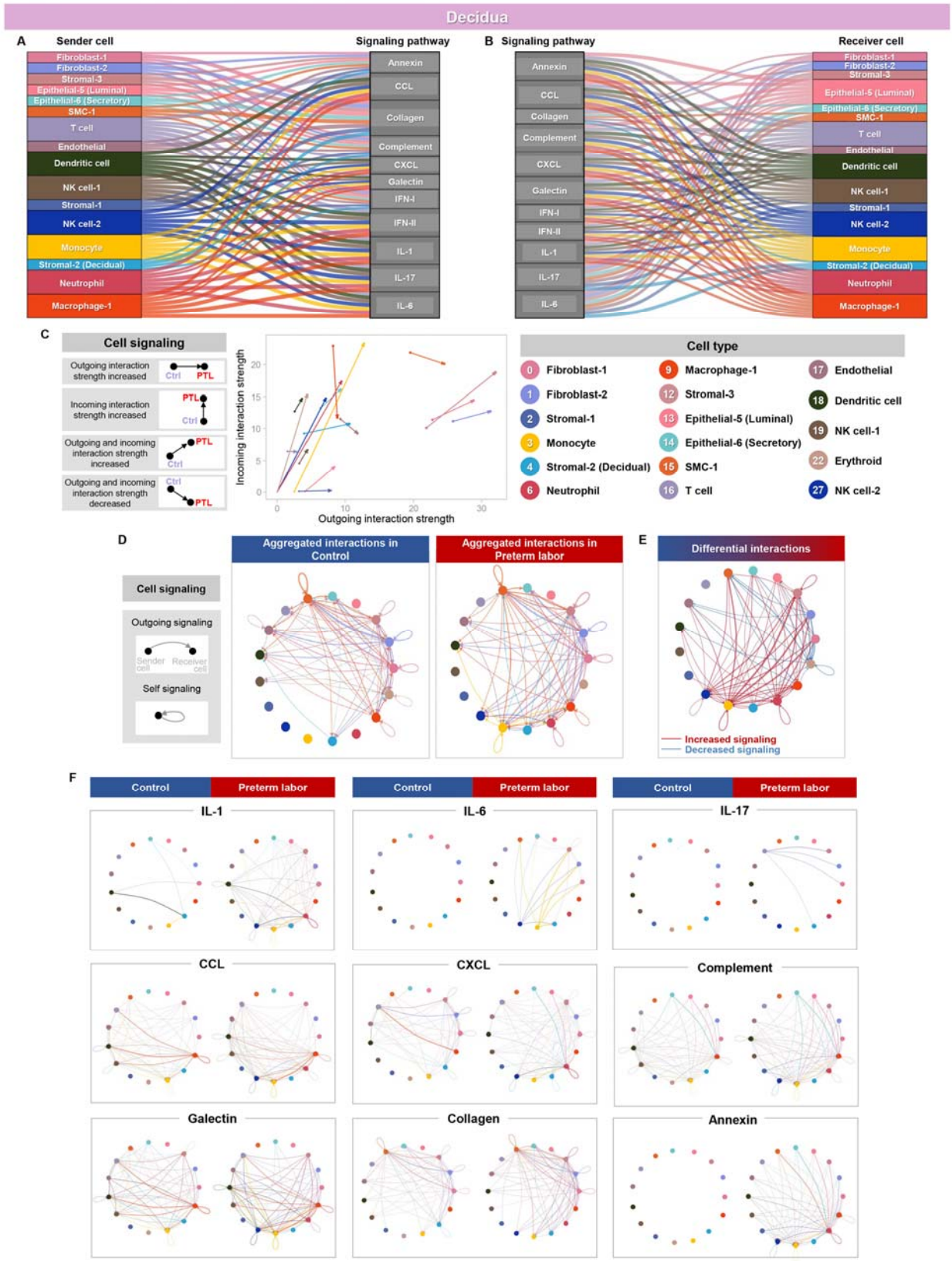

Figure 6. Cellular interactions in the decidua during preterm labor. **(A-B)** Alluvial plots

1380 showing the roles of specific cell types as senders or receivers of preterm labor-associated
1381 signaling in the decidua based on 11 enriched signaling pathways comparing the overall
1382 information flow within networks between preterm labor and control derived from CellChat (see
1383 figure supplement 4B for all pathways). Connecting lines are color-coded and represent the
1384 participation of each cell type as senders or receivers of the indicating signaling pathway. Line
1385 thickness is proportional to the strength of interaction. **(C)** Arrow plot showing changes in the
1386 outgoing and incoming interaction strength between preterm labor (point of the arrow) and
1387 control condition (base of the arrow) for specific cell types in the decidua. **(D)** Circle plots
1388 showing the top 25% of aggregated interactions among cell types in the decidua for control and
1389 preterm labor groups. Each node represents a cell type and the interaction is shown by color-
1390 coded lines. **(E)** Circle plot showing the top 25% increased (red) or decreased (blue) signaling
1391 interactions in the decidua in preterm labor compared to controls. **(F)** Circle plots representing
1392 the top 25% decidual cell-cell communications inferred for the IL-1, IL-6, IL-17, CCL, CXCL,
1393 Complement, Galectin, Collagen, and Annexin pathways for the control and preterm labor
1394 groups. Abbreviations used: SMC, smooth muscle cell; NK cell, natural killer cell.
1395
1396

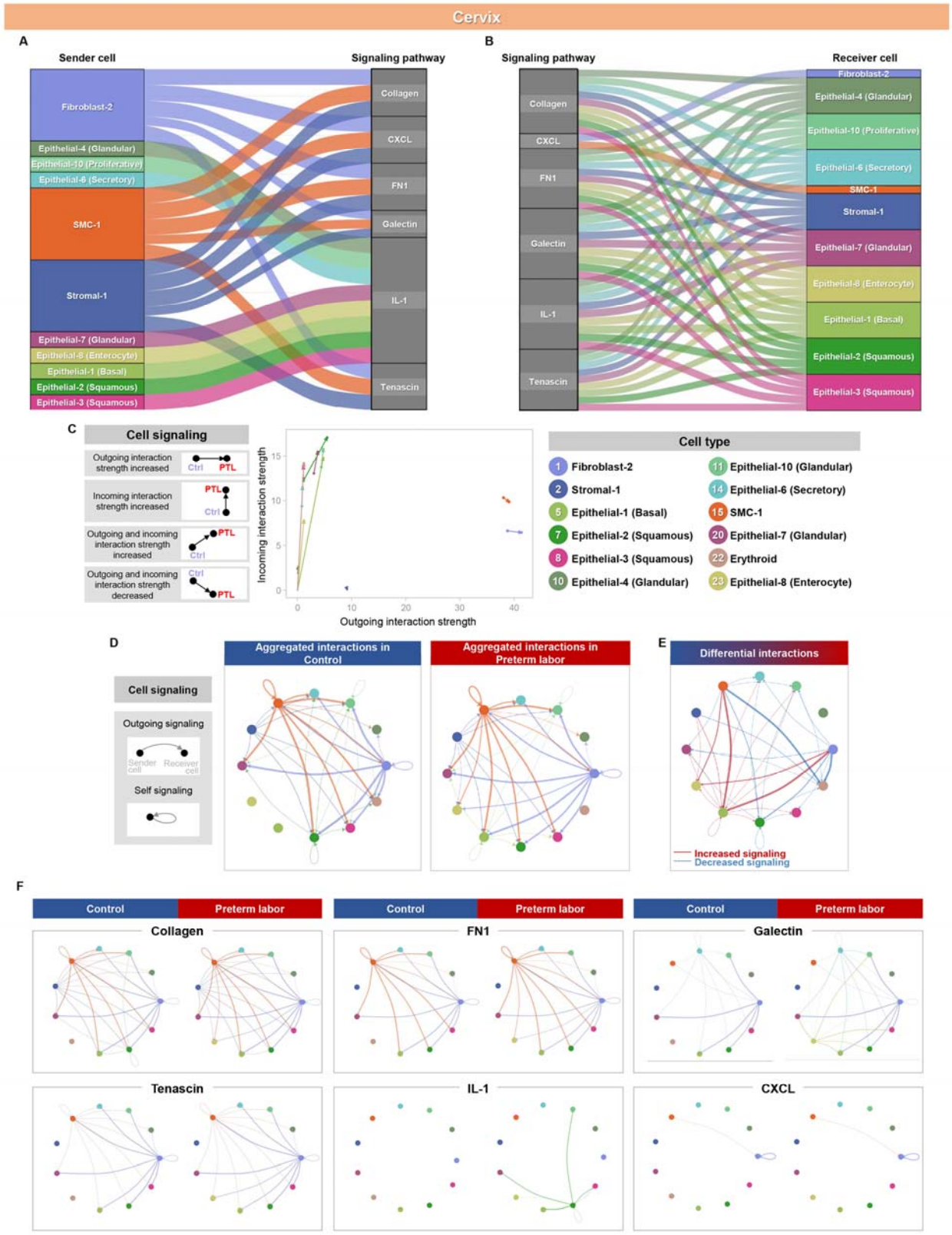

Figure 7. Cellular interactions in the cervix during preterm labor. **(A-B)** Alluvial plots

showing the roles of specific cell types as senders or receivers of preterm labor-associated signaling in the cervix based on selected enriched signaling pathways (see figure supplement 5B for all pathways). Connecting lines are color-coded and represent the participation of each cell type as senders or receivers of the indicating signaling pathway. Line thickness is proportional to the strength of interaction. **(C)** Arrow plot showing changes in the strength of outgoing and incoming interactions between preterm labor (point of the arrow) and control (base of the arrow) for specific cell types in the cervix. **(D)** Circle plots showing the top 25% of aggregated interactions among cell types in the cervix for control and preterm labor groups. Each node represents a cell type and the interaction is shown by color-coded lines. **(E)** Circle plot showing the top 25% increased (red) or decreased (blue) signaling interactions in the cervix in preterm labor compared to controls. **(F)** Circle plots representing the top 25% cervical cell-cell communications inferred for the Collagen, FN1, Galectin, Tenascin, IL-1, and CXCL pathways for the control and preterm labor groups. Abbreviations used: SMC, smooth muscle cell; NK cell, natural killer cell.

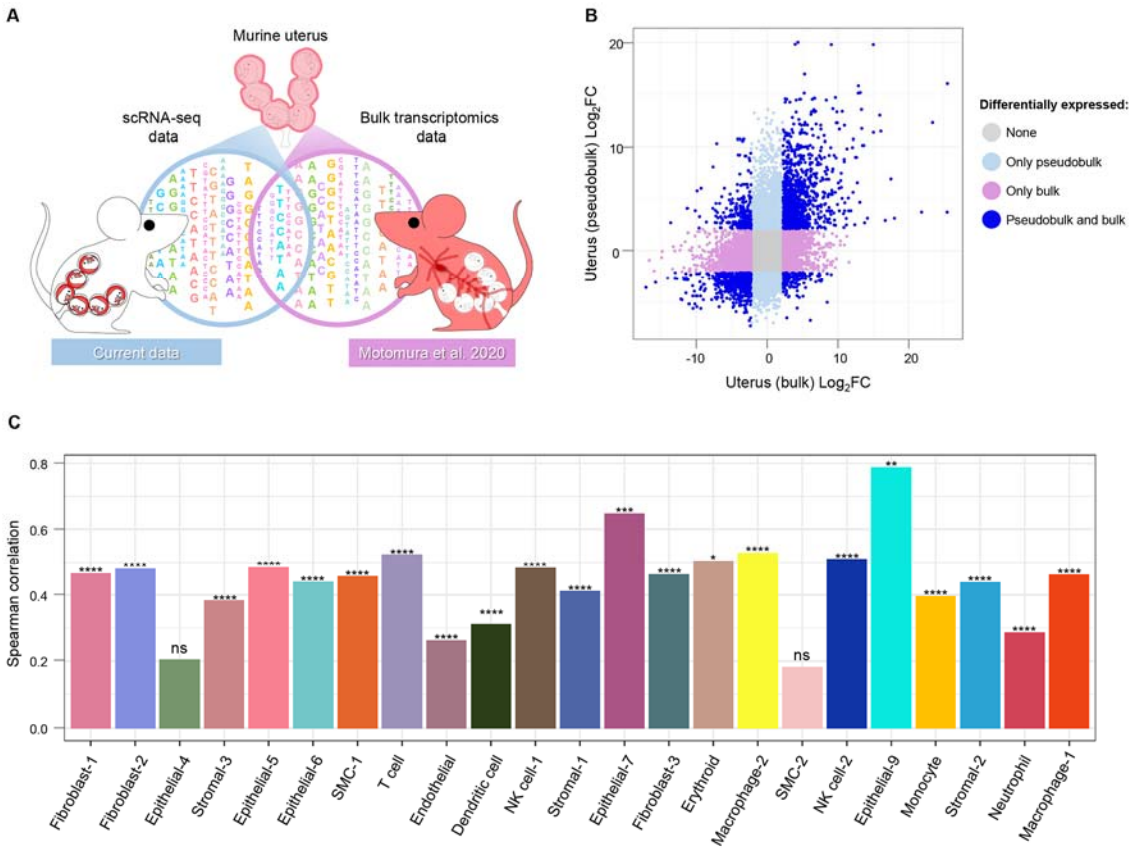

Figure 8. Comparative analysis of the effects of preterm labor induced by local or systemic inflammation. (A) Representative illustration showing the comparative analysis of preterm labor-associated differential gene expression in the uterine tissues when preterm labor is induced by local [single-cell RNA-sequencing (scRNA-seq) (n = 4 in preterm labor; n = 4 control) analyzed as pseudobulk] or systemic inflammation [bulk microarray analysis (n = 9 in preterm labor, n = 10 control), as previously reported (Motomura et al. 2020)]. **(B)** Scatter plot showing the $\log_2$(Fold change; FC) associated with preterm labor derived from pseudo-bulk scRNA-seq (y-axis) or bulk microarray analysis (x-axis) by cell type. Differentially expressed genes (DEGs) ($q < 0.1$) were obtained using only scRNA-seq (light blue) or bulk analysis (lavender), were shared between scRNA-seq and bulk analysis (dark blue), or were not differentially expressed in either dataset (gray). Correlations between datasets were determined using a two-sided

1427 Spearman's correlation test for the subset of DEGs obtained from the pseudo-bulk single cell
1428 analysis. **(C)** Bar plot showing correlations between $\log_2$(FC) of preterm labor-associated DEGs
1429 between cell type-specific scRNA-seq and bulk transcriptomic analysis using 2-sided
1430 Spearman's correlation tests (for the subset of DEGs in each scRNA-seq-derived cell type). P-
1431 values are considered significant when $p < 0.05$. * $p \leq 0.05$, ** $p \leq 0.01$, *** $p \leq 0.001$, **** $p \leq$
1432 0.0001. Abbreviations used: NS, not significant; SMC, smooth muscle cell; NK cell, natural
1433 killer cell.
1434
1435

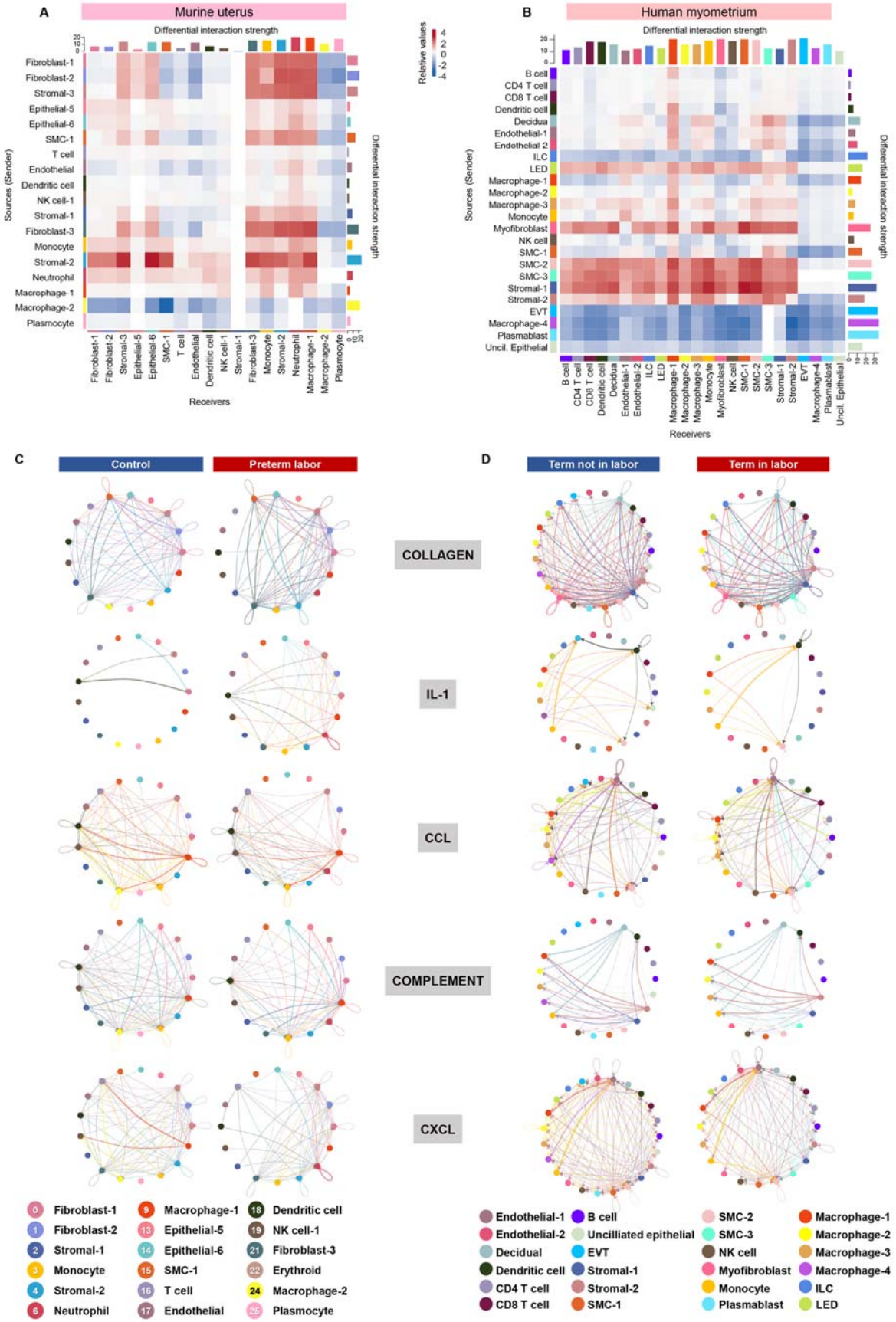
A
Murine uterus
Differential interaction strength
Relative values
Sources (Sender)
Receivers
Differential interaction strength
Fibroblast-1
Fibroblast-2
Stromal-3
Epithelial-5
Epithelial-6
SMC-1
T cell
Endothelial
Dendritic cell
NK cell-1
Stromal-1
Fibroblast-3
Monocyte
Stromal-2
Neutrophil
Macrophage-1
Macrophage-2
Plasmocyte
B
Human myometrium
Differential interaction strength
Sources (Sender)
Receivers
Differential interaction strength
B cell
CD4 T cell
CD8 T cell
Dendritic cell
Decidua
Endothelial-1
Endothelial-2
ILC
LED
Macrophage-1
Macrophage-2
Macrophage-3
Monocyte
Myofibroblast
NK cell
SMC-1
SMC-2
SMC-3
Stromal-1
Stromal-2
EVT
Macrophage-4
Plasmablast
Uncil. Epithelial
C
Control
Preterm labor
COLLAGEN
IL-1
CCL
COMPLEMENT
CXCL
D
Term not in labor
Term in labor
0 Fibroblast-1
1 Fibroblast-2
2 Stromal-1
3 Monocyte
4 Stromal-2
6 Neutrophil
9 Macrophage-1
13 Epithelial-5
14 Epithelial-6
15 SMC-1
16 T cell
17 Endothelial
18 Dendritic cell
19 NK cell-1
21 Fibroblast-3
22 Erythroid
24 Macrophage-2
25 Plasmocyte
Endothelial-1
Endothelial-2
Decidual
Dendritic cell
CD4 T cell
CD8 T cell
B cell
Uncilliated epithelial
EVT
Stromal-1
Stromal-2
SMC-1
SMC-2
SMC-3
NK cell
Myofibroblast
Monocyte
Plasmablast
Macrophage-1
Macrophage-2
Macrophage-3
Macrophage-4
ILC
LED

1436

1437 **Figure 9. Comparison of preterm labor-associated changes in the murine uterus and term**
1438 **labor-associated changes in the human myometrium. (A)** Heatmap showing the differential
1439 interaction strength among cell types in the murine uterus with preterm labor. Red and blue
1440 shading indicate increased or decreased signaling, respectively, in preterm labor compared to
1441 control. **(B)** Heatmap showing the differential interaction strength among cell types in the human
1442 myometrium with term labor. Red and blue shading indicate increased or decreased signaling,
1443 respectively, in term labor compared to term without labor. **(C)** Circle plots representing the top
1444 25% murine uterine cell-cell communications inferred for the Collagen, IL-1, CCL,
1445 Complement, and CXCL pathways for the control and preterm labor groups. **(D)** Circle plots
1446 representing the top 25% human myometrial cell-cell communications inferred for the Collagen,
1447 IL-1, CCL, Complement, and CXCL pathways for the control and preterm labor groups.
1448 Abbreviations used: SMC, smooth muscle cell; NK cell, natural killer cell; EVT, extravillous
1449 trophoblast; ILC, innate lymphoid cell; LED, lymphoid endothelial decidual cell.

1450 **Supplementary Figure Legends**

1451 **Figure 1&2-figure supplement 1. Leukocyte infiltration in the uterus, decidua, and cervix**
1452 **of control mice. (A-C)** Representative Movat pentachrome staining images of the uterus,
1453 decidua, and cervix from control (top row) and preterm labor (bottom row) mice. Red staining
1454 indicates muscle/fibrin, dark purple staining indicates elastic fibers, blue staining indicates
1455 mucin, and yellow indicates collagen/reticular fibers. Nuclei appear as dark blue/black. Whole-
1456 slide images taken at (top row, left to right) 3.7X, 2.9X, and 3.2X; (bottom row, left to right) 4X,
1457 4.9X, and 3.1X (scale bars = 300μm). Zoomed images were all taken at 20X magnification (scale
1458 bars = 50μm). **(D-F)** Representative merged images showing the co-localized
1459 immunofluorescence detection of neutrophils (Ly6G+ cells, pink), monocytes (Ly6C+ cells,
1460 cyan), and macrophages (F4/80+ cells, red) in the uterus, decidua, and cervix of control mice
1461 only (n = 3). Nuclear staining is shown in blue (4',6-diamidino-2-phenylindole; DAPI). Images
1462 were taken at 20X magnification. Scale bar = 100μm.

1463

1464 **Figure 4-figure supplement 2. The uterus and decidua share enrichment of biological**
1465 **processes in preterm labor.** Cluster profiler dot plots showing the Gene Ontology (GO)
1466 biological processes enriched with preterm labor in **(A)** Stromal-1 and Stromal-2, **(B)** Stromal-3
1467 and Fibroblast-1, **(C)** Fibroblast-2 and Fibroblast-3, and **(D)** Endothelial cells in the uterus and
1468 decidua. The size and color of each dot represent gene ratio and significance level, respectively.
1469 A 1-sided Fisher's exact test was used.

1470

1471 **Figure 5-figure supplement 3. Preterm labor-associated enrichment of signaling pathways**
1472 **in uterine cell types. (A)** Heatmap showing correlations among uterine cell types where red and

1473 white blocks signify increased and decreased correlation, respectively. Pearson correlation
1474 method was used. **(B)** Bar plots showing the comparison between the overall information flow
1475 (sum of the communication probability among cell types in the inferred cell-cell network) in
1476 each signaling pathway in the uterus of control mice (blue bars/pathway names) or mice with
1477 preterm labor (red bars/pathway names). The signaling pathways colored red are enriched in
1478 preterm labor, and those colored blue enriched in the control. Abbreviations used: SMC, smooth
1479 muscle cell; NK cell, natural killer cell.

1480

1481 **Figure 6-figure supplement 4. Preterm labor-induced changes in interaction between**
1482 **decidual cell types. (A)** Heatmap showing correlations among decidual cell types where red and
1483 white blocks signify increased and decreased correlation, respectively. Pearson correlation
1484 method was used. **(B)** Bar plots showing the comparison between the overall information flow
1485 (sum of the communication probability among cell types in the inferred cell-cell network) in
1486 each signaling pathway in the decidua of control mice (blue bars/pathway names) or mice with
1487 preterm labor (red bars/pathway names). The signaling pathways colored red are enriched in
1488 preterm labor, and those colored blue enriched in the control. Abbreviations used: SMC, smooth
1489 muscle cell; NK cell, natural killer cell.

1490

1491 **Figure 7-figure supplement 5. Preterm labor-induced changes in interaction between**
1492 **cervical cell types. (A)** Heatmap showing correlations among cervical cell types where red and
1493 white blocks signify increased and decreased correlation, respectively. Pearson correlation
1494 method was used. **(B)** Bar plots showing the comparison between the overall information flow
1495 (sum of the communication probability among cell types in the inferred cell-cell network) in

1496 each signaling pathway in the cervix of control mice (blue bars/pathway names) or mice with
1497 preterm labor (red bars/pathway names). The signaling pathways colored red are enriched in
1498 preterm labor, and those colored blue enriched in the control.
1499
1500 **Figure 9-figure supplement 6. Labor-associated signaling in the human myometrium**
1501 **partially overlaps with preterm labor-associated changes in the murine uterus. (A)** Circle
1502 plots showing the top the aggregated interactions among cell types in the myometrium from
1503 humans without (left) or with labor at term (right). Each node represents a cell type and the
1504 interaction is shown by lines color-coded based on the sender cell. Representation of aggregated
1505 interactions with $p < 0.05$ using cell chat. **(B)** Circle plot showing the increased (red) or
1506 decreased (blue) signaling interactions in the human myometrium in labor compared to controls
1507 without labor. Representation of top 25% differential interaction strength. **(C)** Venn diagram
1508 showing the overlap in signaling pathways with the most number of differentially expressed
1509 genes ($q < 0.1$) between the murine uterus in preterm labor (left circle, pink) and the human
1510 myometrium in term labor (right circle, orange). Shared labor- and inflammation-associated
1511 pathways are highlighted in red. Abbreviations used: SMC, smooth muscle cell; NK cell, natural
1512 killer cell; EVT, extravillous trophoblast; ILC, innate lymphoid cell; LED, lymphoid endothelial
1513 decidual cell.
1514
1515 **Supplementary File Legends**
1516 **Supplementary file 1.** Summary of the number of uterine, decidual, and cervical cells
1517 encapsulated within the 10x Genomics Gel-bead-in-emulsion (GEM). Each row summarizes the
1518 total number of each cell type and split by condition (Control and Preterm labor group)

1519 **Supplementary file 2.** Preterm labor-associated differentially expressed genes in uterine cell
1520 types. The columns represent 1) cell type name or cluster and 2) number of differentially
1521 expressed genes.

1522 **Supplementary file 3.** Preterm labor-associated differentially expressed genes in decidual cell
1523 types. The columns represent 1) cell type name or cluster and 2) number of differentially
1524 expressed genes.

1525 **Supplementary file 4.** Preterm labor-associated differentially expressed genes in cervical cell
1526 types. The columns represent 1) cell type name or cluster and 2) number of differentially
1527 expressed genes.

1528 **Supplementary file 5.** CellChat analysis in uterine cell types. List of signaling pathways, genes
1529 involved in pathways, labor-associated differentially expressed genes (DEGs), cell types with
1530 DEGs, the overall contribution (information flow) in a condition, and the p-value comparing the
1531 overall information flow within the inferred networks between study groups in the uterus.

1532 **Supplementary file 6.** CellChat analysis in decidual cell types. List of signaling pathways from
1533 CellChat, genes involved in pathways, labor-associated differentially expressed genes (DEGs),
1534 cell types with DEGs, the overall contribution (information flow) in a condition, and the p-value
1535 comparing the overall information flow within the inferred networks between study groups in the
1536 decidua.

1537 **Supplementary file 7.** CellChat analysis in cervix cell types. List of signaling pathways from
1538 CellChat, genes involved in pathways, labor-associated differentially expressed genes (DEGs),
1539 cell types with DEGs, the overall contribution (information flow) in a condition, and the p-value
1540 comparing the overall information flow within the inferred networks between study groups in the
1541 cervix.

1542 **Supplementary file 8.** List of marker genes for the identification of cell types in the murine
1543 uterus, decidua and cervix. The columns represent 1) cell type name or cluster, 2) gene symbol,
1544 3) nominal p-value, 4) $\log_2$(Fold change) of the average expression between this cluster and the
1545 rest, 5) pct.1: percentage of cells in this cluster where the feature is detected, 6) pct.2: percentage
1546 of cells in other clusters where the feature is detected, and 7) q-value.

1547 **Supplementary file 9.** Preterm labor-associated differentially expressed genes in murine uterus,
1548 decidua and cervix. The columns represent: 1) gene symbol, 2) baseMean gene baseline
1549 expression as calculated by DESeq2, 3) $\log_2$(Fold change) of the comparison between groups, 4)
1550 standard error estimated for the $\log_2$(Fold change), 5) DESeq2 statistics, 6) nominal p-value, 7)
1551 q-value, 8) tissue, and 9) cell type or cluster.

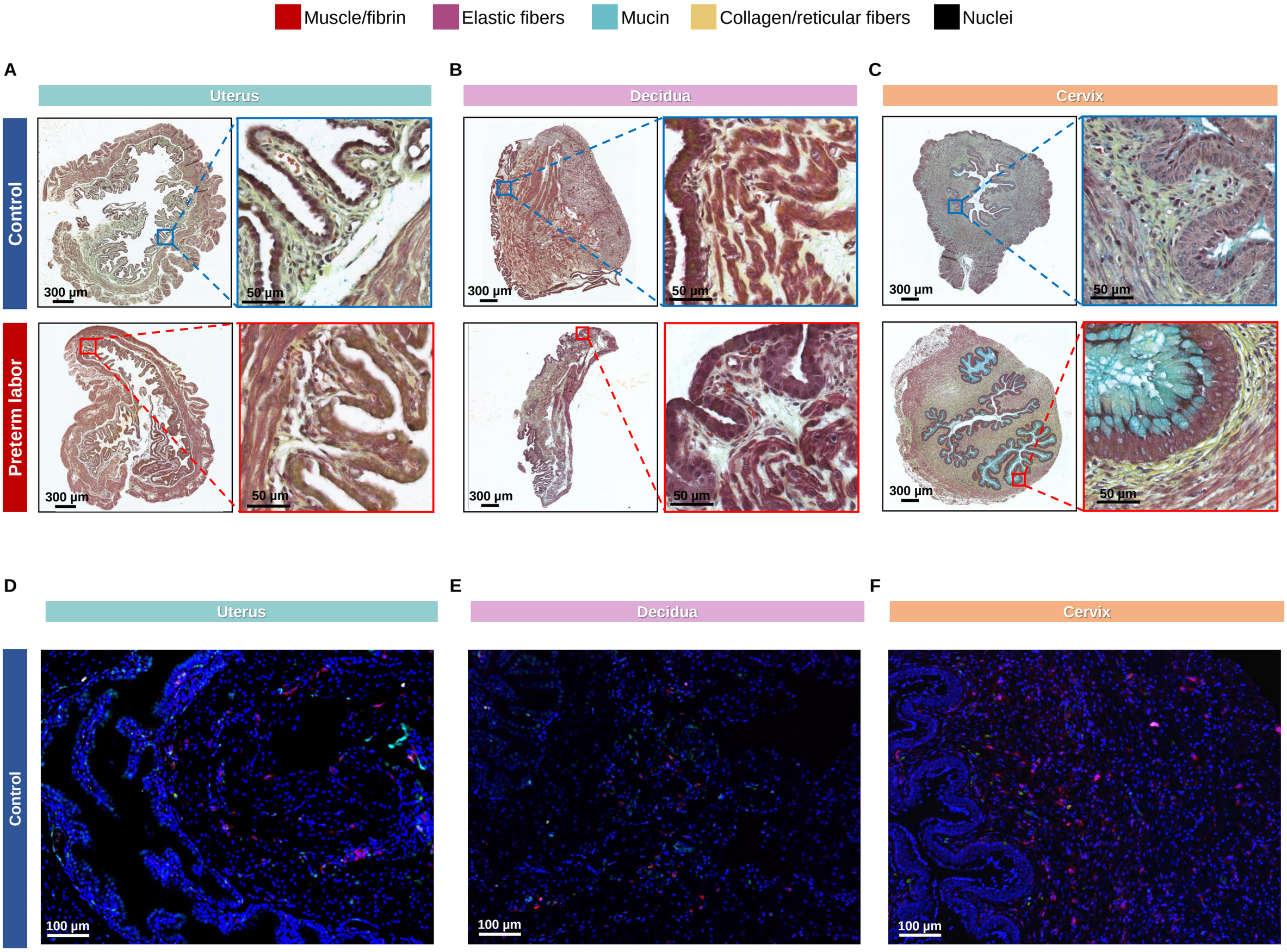

Figure 1&2-figure supplement 1. Leukocyte infiltration in the uterus, decidua, and cervix. (A-C) Representative Movat pentachrome staining images of the uterus, decidua, and cervix from control (top row) and preterm labor (bottom row) mice. Red staining indicates muscle/fibrin, dark purple staining indicates elastic fibers, blue staining indicates mucin, and yellow indicates collagen/reticular fibers. Nuclei appear as dark blue/black. Whole-slide images taken at (top row, left to right) 3.7X, 2.9X, and 3.2X; (bottom row, left to right) 4X, 4.9X, and 3.1X (scale bars = 300µm). Zoomed images were all taken at 20X magnification (scale bars = 50µm). **(D-F)** Representative merged images showing the co-localized immunofluorescence detection of neutrophils (Ly6G+ cells, pink), monocytes (Ly6C+ cells, cyan), and macrophages (F4/80+ cells, red) in the uterus, decidua, and cervix of control mice only (n = 3). Nuclear staining is shown in blue (4',6-diamidino-2-phenylindole; DAPI). Images were taken at 20X magnification. Scale bar = 100µm.

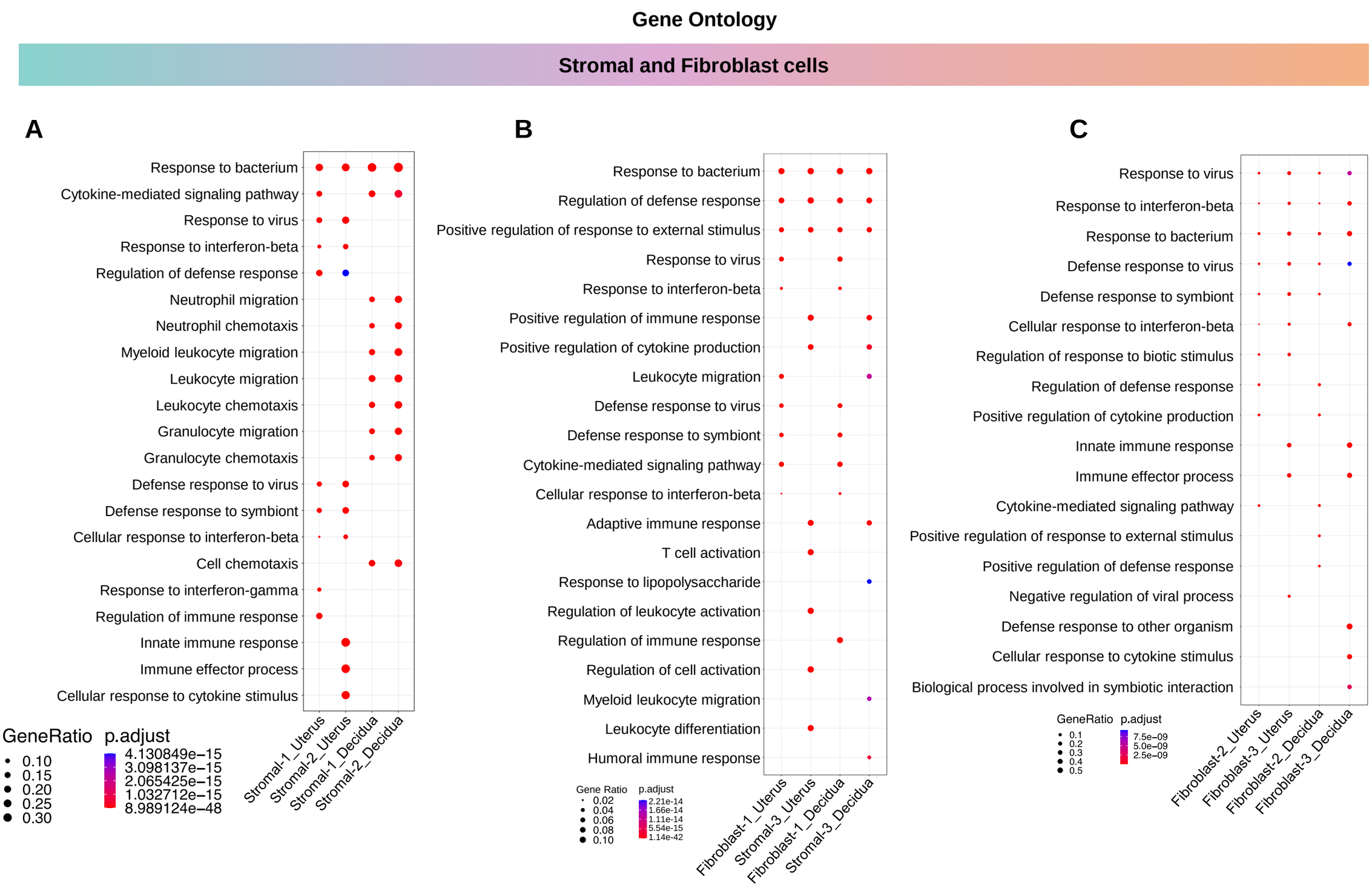

Figure 4-figure supplement 2. The uterus and decidua share enrichment of biological processes in preterm labor. Cluster profiler dot plots showing the Gene Ontology (GO) biological processes enriched with preterm labor in **(A)** Stromal-1 and Stromal-2, **(B)** Stromal-3 and Fibroblast-1, **(C)** Fibroblast-2 and Fibroblast-3, and **(D)** Endothelial cells in the uterus and decidua. The size and color of each dot represent gene ratio and significance level, respectively. A 1-sided Fisher's exact test was used.

Uterus

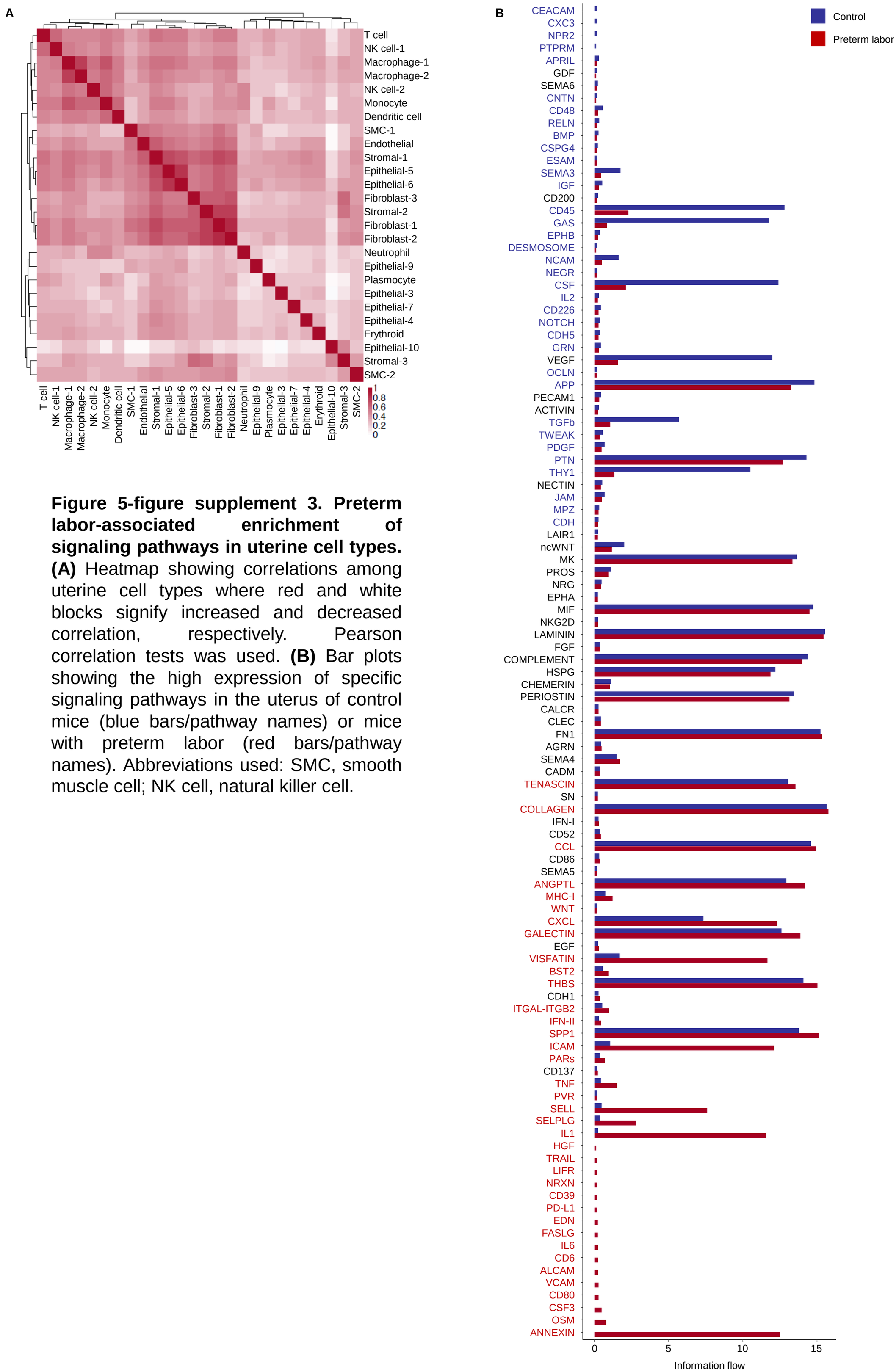

Figure 5-figure supplement 3. Preterm labor-associated enrichment of signaling pathways in uterine cell types. (A) Heatmap showing correlations among uterine cell types where red and white blocks signify increased and decreased correlation, respectively. Pearson correlation tests was used. **(B)** Bar plots showing the high expression of specific signaling pathways in the uterus of control mice (blue bars/pathway names) or mice with preterm labor (red bars/pathway names). Abbreviations used: SMC, smooth muscle cell; NK cell, natural killer cell.

Decidua

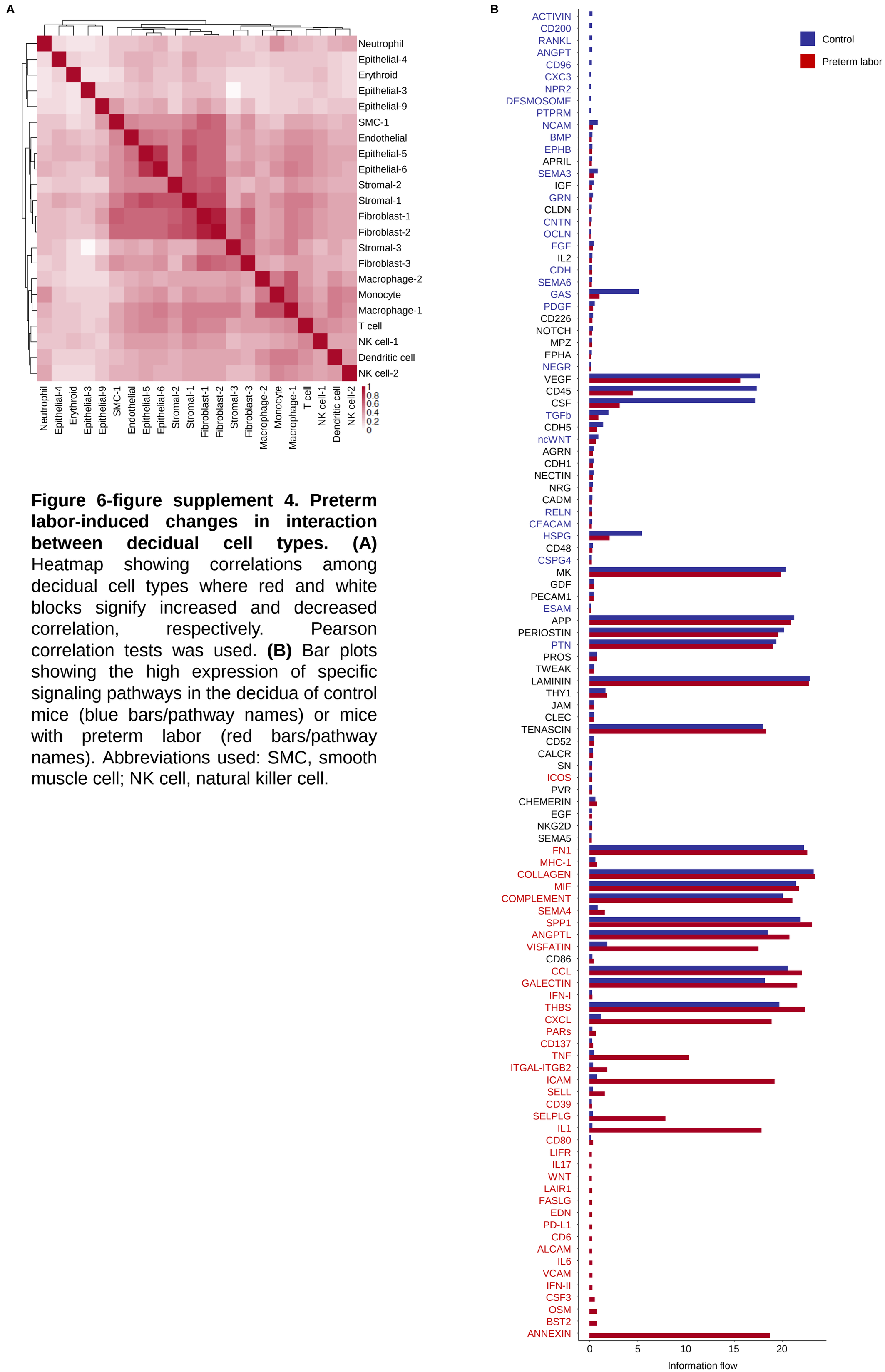

Figure 6-figure supplement 4. Preterm labor-induced changes in interaction between decidual cell types. (A) Heatmap showing correlations among decidual cell types where red and white blocks signify increased and decreased correlation, respectively. Pearson correlation tests was used. **(B)** Bar plots showing the high expression of specific signaling pathways in the decidua of control mice (blue bars/pathway names) or mice with preterm labor (red bars/pathway names). Abbreviations used: SMC, smooth muscle cell; NK cell, natural killer cell.

Cervix

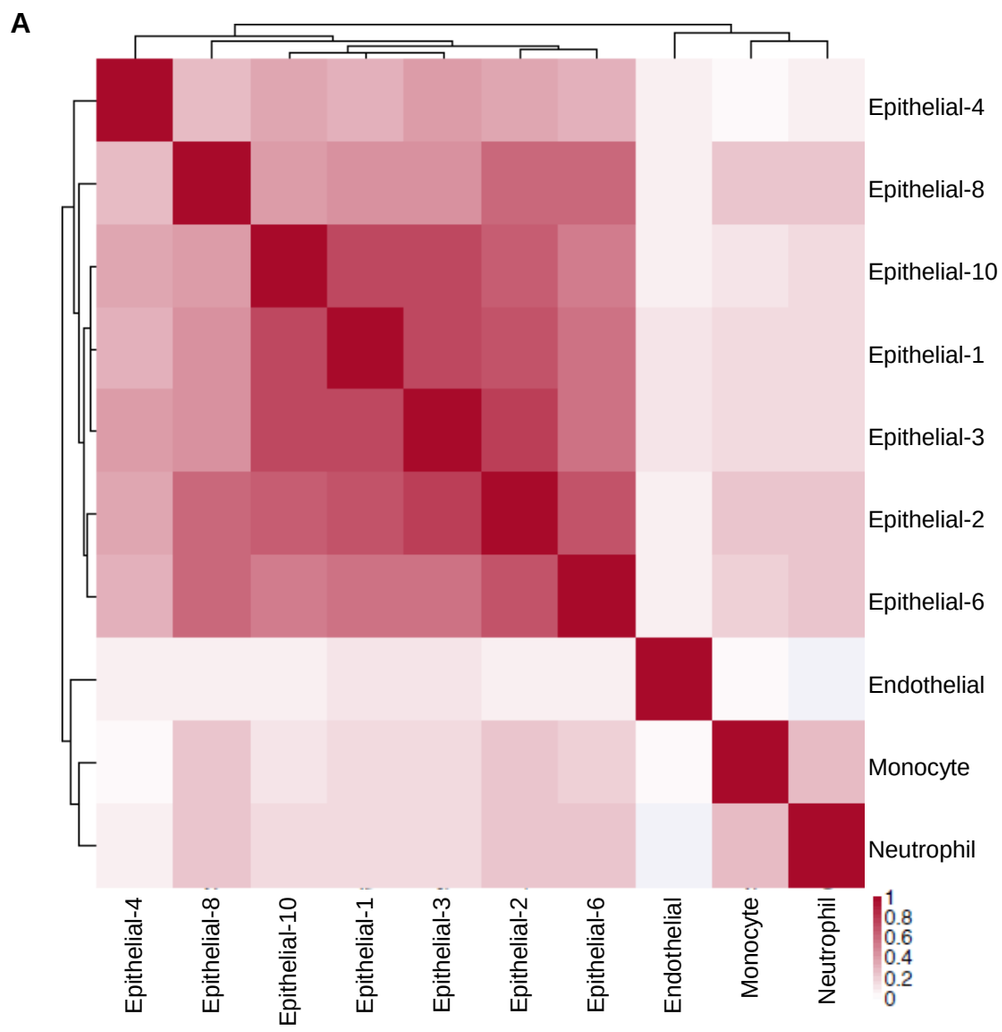

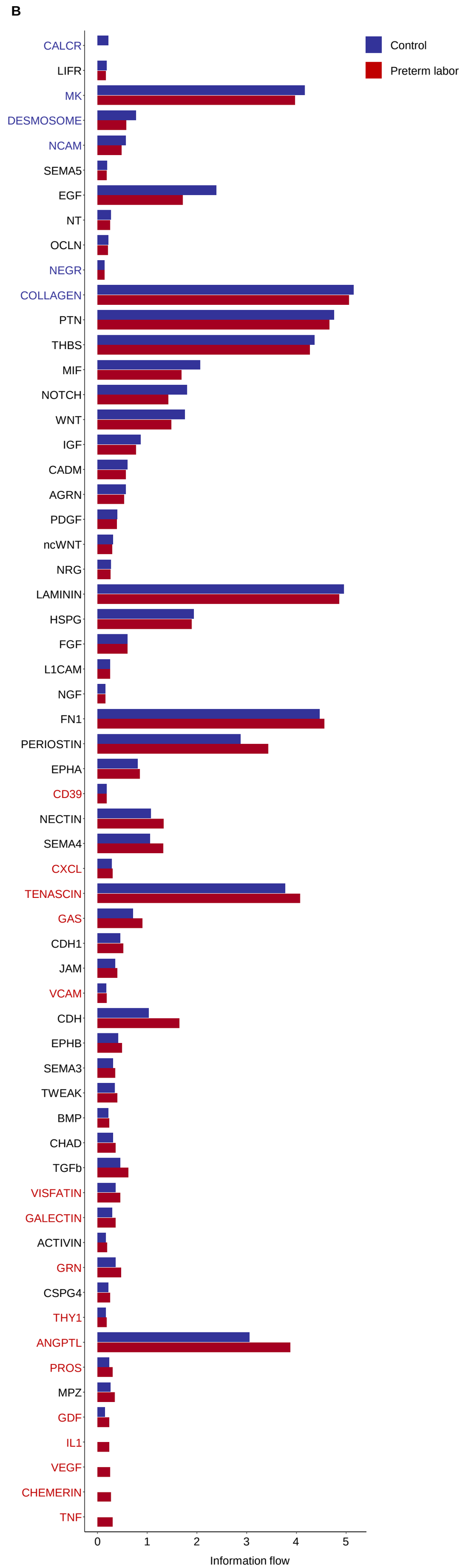

Figure 7-figure supplement 5. Preterm labor-induced changes in interaction between cervical cell types. (A) Heatmap showing correlations among cervical cell types where red and white blocks signify increased and decreased correlation, respectively. Pearson correlation tests was used. **(B)** Bar plots showing the high expression of specific signaling pathways in the cervix of control mice (blue bars/pathway names) or mice with preterm labor (red bars/pathway names).

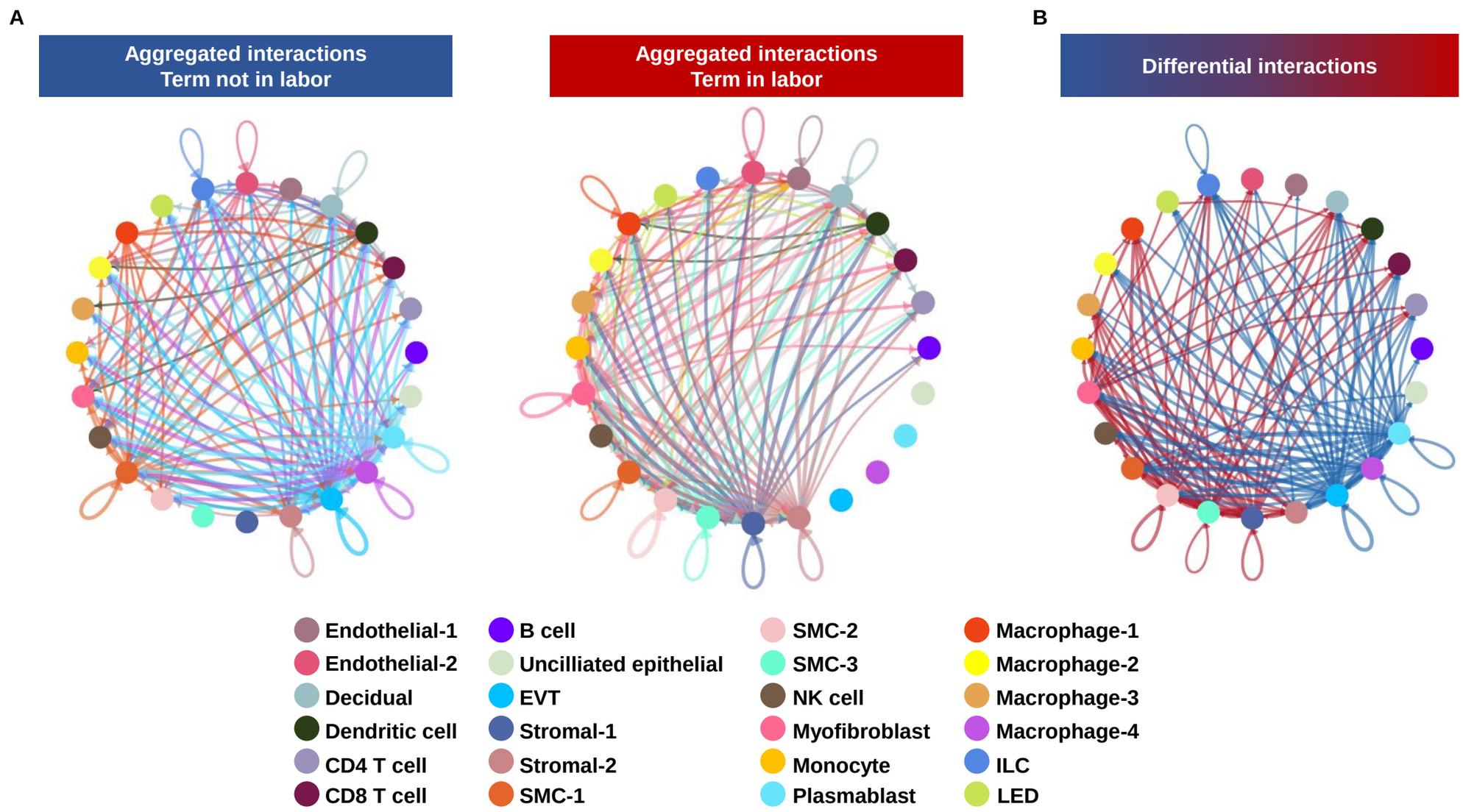

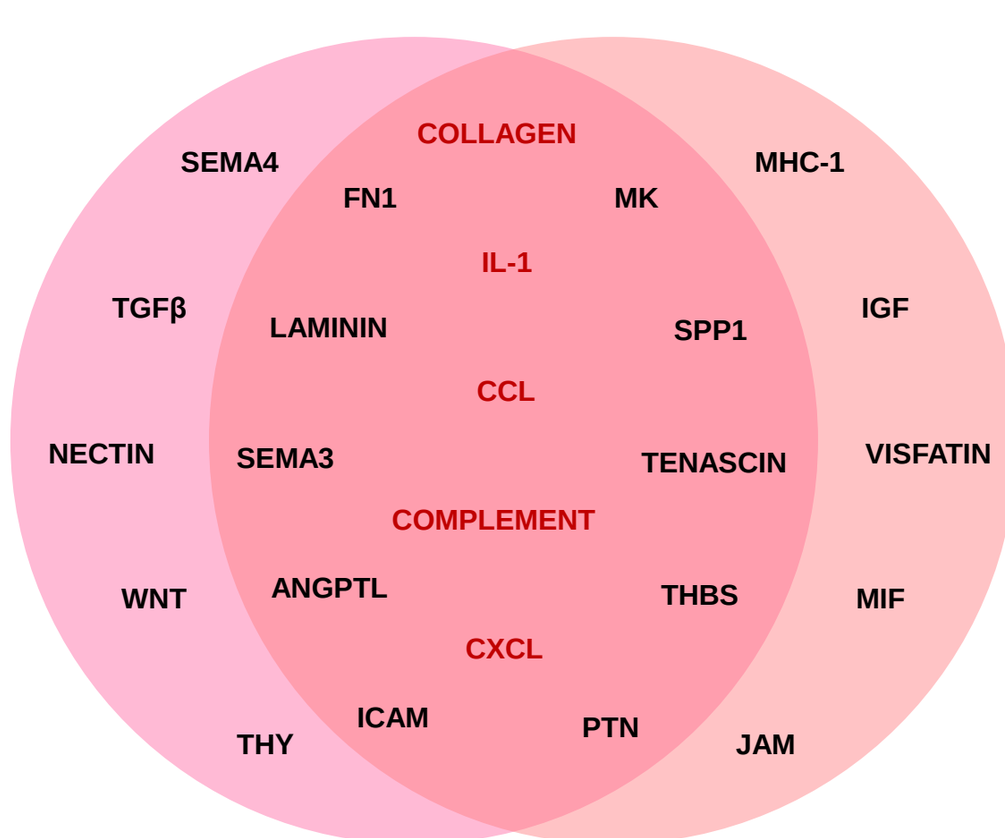

Figure 9-figure supplement 6. Labor-associated signaling in the human myometrium partially overlaps with preterm labor-associated changes in the murine uterus. (A) Circle plots showing the top the aggregated interactions among cell types in the myometrium from humans without (left) or with labor at term (right). Each node represents a cell type and the interaction is shown by lines color-coded based on the sender cell. Representation of aggregated interactions with $p < 0.05$ using cell chat. **(B)** Circle plot showing the increased (red) or decreased (blue) signaling interactions in the human myometrium in labor compared to controls without labor. Representation of top 25% differential interaction strength. **(C)** Venn diagram showing the overlap in upregulated signaling pathways between the murine uterus in preterm labor (left circle, pink) and the human myometrium in term labor (right circle, orange). Shared labor- and inflammation-associated pathways are highlighted in red. Abbreviations used: SMC, smooth muscle cell; NK cell, natural killer cell; EVT, extravillous trophoblast; ILC, innate lymphoid cell; LED, lymphoid endothelial decidual cell.